Exploiting Seasonal Surplus Energy from Geothermal Utilization for Electrical Power Production

Pálmar Sigurðsson

Faculty of Industrial Engineering, Mechanical Engineering and Computer Science
University of Iceland
2016

Exploiting Seasonal Surplus Energy from Geothermal Utilization for Electrical Power Production

Pálmar Sigurðsson

30 ECTS thesis submitted in partial fulfillment of a
Magister Scientiarum degree in Mechanical Engineering

Advisors
Associate Professor Halldór Pálsson
Marta Rós Karlsdóttir
Bjarni Már Júlíusson
Guðmundur Kjartansson

Faculty Representative
Egill Maron Þorbergsson

Faculty of Industrial Engineering, Mechanical Engineering and Computer Science
School of Engineering and Natural Sciences
University of Iceland
Reykjavik, May 2016

Exploiting Seasonal Surplus Energy from Geothermal Utilization for Electrical Power Production

Feasibility Study for Geothermal Bottoming Units

30 ECTS thesis submitted in partial fulfillment of a *Magister Scientiarum* degree in Mechanical Engineering

Faculty of Industrial Engineering, Mechanical Engineering and Computer Science
School of Engineering and Natural Sciences
University of Iceland
VR-II, Hjarðarhagi 2-6
107, Reykjavik
Iceland

Telephone: 525 4000

Bibliographic information:
Pálmar Sigurðsson, 2016, *Exploiting Seasonal Surplus Energy from Geothermal Utilization for Electrical Power Production*, Master's thesis, Faculty of Industrial Engineering, Mechanical Engineering and Computer Science, University of Iceland.

Printing: Háskólaprent
Reykjavik, Iceland, June 2016

Abstract

Operation of geothermal power plants is a well-known subject. However, the interaction between heat and power production from seasonal surplus heat have not been investigated at length. This study focuses on exploiting the surplus heat from geothermal combined heat and power (CHP) plants for electrical power production. Nesjavellir geothermal CHP plant in Iceland was used as a case study but the work was structured so it could be implemented for other cases. District heat production at Nesjavellir is highly dependent on seasonal changes in heat load. The amount of seasonal surplus at Nesjavellir was calculated from present demand and estimated for future scenarios. Static thermodynamic models were constructed and optimized for two different bottoming units with the purpose to produce electrical power from heat with variating availability. The bottoming units in question were an organic Rankine cycle (ORC) and a flashing process with a low pressure turbine (LPT). A preliminary feasibility study was performed for both bottoming units. Changes in environmental impact due to a possible bottoming unit at Nesjavellir were addressed and problems with utilizing the seasonal variating heat mentioned. The results from this study indicate that there is an economical feasible way of exploiting the seasonal surplus for electrical power production.

Útdráttur

Rekstur jarðvarmavirkjana er vel þekkt viðfangsefni. Hins vegar hefur samspilið á milli hitaframleiðslu og raforkuframleiðslu frá umframvarma ekki verið rannsakað ítarlega. Verkefnið fjallar um nýtingu á árstíðabundnum umframvarma frá jarðvarmaverum til framleiðlsu á raforku. Nesjavellir voru teknir til umfjöllunar en verkefnið sjálft var byggt upp með þeim hætti að hægt væri að taka annað jarðvarmaver til skoðunar. Hitaframleiðsla frá Nesjavöllum er háð árstíðabundnum breytingum á hitaþörf. Framboð á umframvarma á Nesjavöllum var reiknað samkvæmt núverandi hitaþörf. Einnig var spáð fyrir um framtíðarmagn af umframvarma. Byggð voru varmafræðileg bestunarlíkön fyrir tvo vinnuhringi sem framleiða raforku úr breytilegu framboði á varma. Þeir vinnuhringir sem teknir voru fyrir eru Rankine tvívökvahringrás (e. organic Rankine cycle) og hvellsuðuferli með lágþrýstivél (e. low pressure turbine cycle). Fyrsta stigs reikningar á hagkvæmni voru gerðir fyrir báða vinnuhringi. Umhverfisáhrif á Nesjavöllum vegna tilkomu nýs vinnuhrings voru tekin fyrir, sem og hugsanleg vandamál tengd nýtingu á árstíðabundnum umframvarma. Niðurstöður verkefnisins gefa til kynna að hægt sé að nýta umframvarma á Nesjavöllum til raforkuframleiðslu á hagkvæman máta.

Table of Contents

List of Figures

List of Tables

Nomenclature

Latin Letters

A	Heat transfer area [m^2 or ft^2]
A_{eq}	Equal-amount money transaction [ISK or US$]
Avail.	Availability [% of year]
C	Cost [ISK or US$]
CAPEX	Capital expenditure [ISK or US$]
CHP	Combined heat and power
CRF	Capital recovery factor [-]
D	Diameter [m or ft]
DH	District heating
$\dot{E}$	Exergy [kJ/s or kW]
e	specific exergy [kJ/kg]
e.g.	la. exempli gratia, e. for example
H	Pump head [m or ft]
h	Specific enthalpy [kJ/kg]
i	Interest rate or rate of return [-]
LC	Levelized cost of electricity [ISK/yr.]
LPT	Low pressure turbine
$\dot{m}$	Mass flow rate [kg/s]
M	Molar mass [kg/mol]
OPEX	Operational and maintenance expenditure [IKS/yr. or US$/yr.]
ORC	Organic Rankine cycle
P	Power [W or horse power]
p	Pressure [Pa, bar or psi]
Q	Flow rate [kg/s or gal/min]
RoR	Rate of return [-]
S	Size factor
s	Specific entropy [kJ/(kg K)]
T	Temperature [°C or K]
T&S	Tube and shell
U	Overall heat transfer coefficient [$W/(m^2 K)$]
v	Velocity [m/s or ft/s]
W	Energy [kWh or GWh]
We	Weight [kg or lbs]
x	Mass fraction [-]
X	Size or capacity

Greek Letters

η	Isentropic efficiency [-]
η_{II}	Second law efficiency [-]
η_{th} & η_I	Thermal or first law efficiency [-]
υ	Specific volume [m^3/kg]
α	Scaling component
Δ	Difference
ρ	Density [kg/m^3]
ϕ	Relative humidity [-]

ω	Humidity ratio [-]

Subscript

a	Air and atmospheric
B	Base
bo	Boiler
br	Brine
c	Consumption
ca	Cooling air
cond	Condenser
ct	Cooling tower
cw	Cooling water
e	Electrical
em	Electric motor
eq	Equipment and Equal-amount
fan	Fan
FiH	Fixed head heat exchanger
FlH	Floating head heat exchanger
g	Gauge
he	Heater
high	High value
hor	Horizontal
is	Isentropic
KV	Kettle vaporizer heat exchanger
lm	Logarithmic mean
low	Low value
M	Material factor
max	Maximum value
min	Minimum value
net & tot	Net and total
P	Pressure factor
pu	Pump
re	Recuperator
s	Saturation
sep	Separator
T	Type factor
T1 & T2	Turbine 1 and Turbine 2
th	Thermal
turb	Turbine
UT	U-tube heat exchanger
ver	Vertical
w	Water
wf	Working fluid

Acknowledgements

Halldór Pálsson at University of Iceland

Marta Rós Karlsdóttir, Bjarni Már Júlíusson and Guðmundur Kjartansson at ON Power

Landsvirkjun Energy Research Fund for funding the project

Sigrún Nanna Karlsdóttir, Yngvi Guðmundsson, Páll Valdimarsson and Ingvi Gunnarsson

David Pallarès at Chalmers University of Technology

The coordinators of the ISEE Nordic Master's program and the Winter Schools

Sara Matthíasdóttir and Þorri Matthías Pálmarsson

Sigurður Jón Jónsson and Guðný Jónsdóttir

Jón Otti Sigurðsson, Valborg Guðmundsdóttir, Signý Alda and Iðunn Brynja

Þorsteinn Sigurðsson and Kisi

Matti Grabo and the Gothenburg crew

The finest of Húsahverfi and the Council of Elders

1 Introduction

For centuries mankind has been utilizing geothermal energy for domestic and industrial use, with electrical power production being most common (Dickson & Fanelli, 2013). There are three main types of geothermal power plants: dry steam power stations, flash steam power stations and binary or twin-fluid power stations (DiPippo, 2012). As of the beginning of 2016, installed generating capacity of geothermal worldwide is 13.3 GW_e with more than 42% of the production coming from single-flash geothermal power plants (Matek, 2016). Geothermal steam is preferred for electricity production while geothermal waters, or brine, can be used for electricity production by binary units, heating, farming or agriculture (Axelsson, 2015).

Geothermal combined heat and power (CHP) plants with variating heat demand have the possibility of increased power production during seasons of low heat demand. An option for increased electrical power production from CHP plants is a bottoming cycle which utilizes thermal energy from separated brine (DiPippo, 2012). With sufficient seasonal surplus available, the bottoming cycle could generate electricity during periods of low heat demand. When the demand would increase again, the thermal energy would be utilized for heat production and the power generating bottoming cycle recede (Júlíusson, Kjartansson, & Karlsdóttir, 2016).

A well-known geothermal single-flash CHP plant in Iceland is considered in this study but the work was structured so it could be implemented for other scenarios. The power plant chosen is Nesjavellir plant, located in Southwestern part of Iceland, 35 km West of Reykjavík. The production capacity at Nesjavellir is 120 MW_e and 300 MW_{th} of hot water used for district heating (Kjartansson, 2015). The heat produced at Nesjavellir is utilized by Reykjavík and surrounding municipalities while electricity is produced for both industry and domestic usage. The demand for electricity from the power plant is relatively stable throughout the year but the demand for heat is highly dependent on the seasonal variations (Júlíusson et al., 2016).

When the heat demand is low, e.g. during summer time, a lot of the separated liquid, or brine, is not utilized for production of district heating water for Reykjavík. Instead the brine is either pumped back into a shallow reservoir below the groundwater reservoir or decreased in pressure and disposed of above ground. In both cases the overall performance of the power plant decreases during periods of low heat demand (Zarandi & Ívarsson, 2010). By utilizing the surplus heat, the overall energy efficiency of the plant would increase. At the same time surface disposal from the plant would decrease. The most common types of power generating bottoming cycles are flash steam cycles at a lower pressure and binary cycles (DiPippo, 2012). The bottoming cycles considered for this study were an organic Rankine cycle and a low pressure flash steam cycle.

Hellisheiði is a geothermal CHP plant located close to Nesjavellir. There is an interconnection between heat production for district heating water at Nesjavellir and Hellisheiði (Kjartansson, 2010). Therefore, Hellisheiði could produce more heat to have more seasonal surplus heat available at Nesjavellir for further utilization. In the first part of

this study, the interconnection between Nesjavellir and Hellisheiði is investigated in detail. From that information, the amount of available surplus heat at Nesjavellir during different periods is calculated. The drawbacks of utilizing the brine are also investigated.

In the second part of the project, two different bottoming cycles are simulated and optimized. Thermodynamic models of a low pressure flash steam cycle and an organic Rankine cycle are formulated in MATLAB®. The thermodynamic properties are calculated with CoolProp (Bell et al., 2014). The models are optimized with a built-in multivariable function in MATLAB® called fmincon (MATLAB, 2014). A preliminary feasibility study is done for both cycles following with a short environmental impact study due to the reason that Nesjavellir is located close to Þingvellir, a national park, where very strict environmental laws apply. Certain assumptions are made during the modelling that must be kept in mind when interpreting the results.

Ways of improving the energy efficiency for geothermal power plants are well known but the interaction between heat and power production from seasonal surplus heat have not been investigated at length. This interaction increases the complexity for utilization and creates uncertainty whether it is economically feasible to produce electricity from surplus heat due to seasonal changes. When heat demand increases, the electricity production from surplus heat would have to recede for the heat production. If utilization would be economically feasible, it would increase the overall energy efficiency of the power plant during periods of low heat demand and likely decrease the environmental impact from the power plant due to less heat disposal above ground.

The study is structured as follows. The second chapter describes methods of utilizations and Nesjavellir geothermal CHP is studied in more detail. The third chapter goes into thermodynamic calculations for an ORC and LPT cycle and the capital and operational expenditures are estimated. The fourth chapter describes the optimization methods used to optimize both bottoming cycles and assumptions made in the study. The fifth chapter depicts and lists results of thermodynamic simulations and optimizations. The final chapter is a summation of results, conclusion and includes suggestions for future work.

2 Geothermal Energy

Geothermal energy is thermal energy contained within the Earth. Roughly 87.5% of the heat is generated from the decay of long-lived radioactive isotopes within the mantle and the crust. The relative proportion of these radioactive elements is much higher in the crust than in the mantle. Even though the mass of the mantle is approximately 200 times the mass of the crust, the heat generation from the mantle is only 2.4 times the heat generation of the crust (Guðmundsson, 2015). Although geothermal energy is a vast amount of heat stored within the Earth, the term is mostly used for the portion of the energy which is recoverable and exploitable by mankind (Dickson & Fanelli, 2013).

Geothermal energy has been utilized by mankind for centuries. Historians date the beginning of direct utilization of geothermal waters back to approximately 8000 BC whereas the first attempt at generating electricity from geothermal steam dates back to 1904. The attempt was made at Larderello in Southern Tuscany, Italy, by extracting steam through shallow wells drilled in the area and utilizing it to generate electrical energy. Apart from many obstacles, the attempt was a commercial success, indicating the industrial value of geothermal energy (Dickson & Fanelli, 2013). Nowadays, geothermal energy is mainly utilized by drilling wells, extracting fluid from the reservoir and generating electricity, producing heat or both. Geothermal steam is preferred for electricity production while geothermal waters, or brine, can be used for electricity production, heating, farming and agriculture (Axelsson, 2015).

2.1 Geothermal Utilization

Geothermal energy is mainly used for electric power and heat production. All electricity generating geothermal power plants are categorized into three main groups; dry steam power stations, flash steam power stations and binary or twin-fluid power stations. Geothermal power plants which produce both electrical energy and thermal energy are called combined heat and power plants (DiPippo, 2012).

2.1.1 Dry and Flash Steam Systems

Dry steam and flashed steam power cycles are similar and therefore grouped together. The diagram for a dry steam power plant is similar to a single-flash power plant, see Figure 2.1, with the exception that liquid coming from the gathering system is steam. The pressure valve and separator are not needed for the dry steam system, as mentioned above. With that in mind, describing the single-flash steam cycle will suffice.

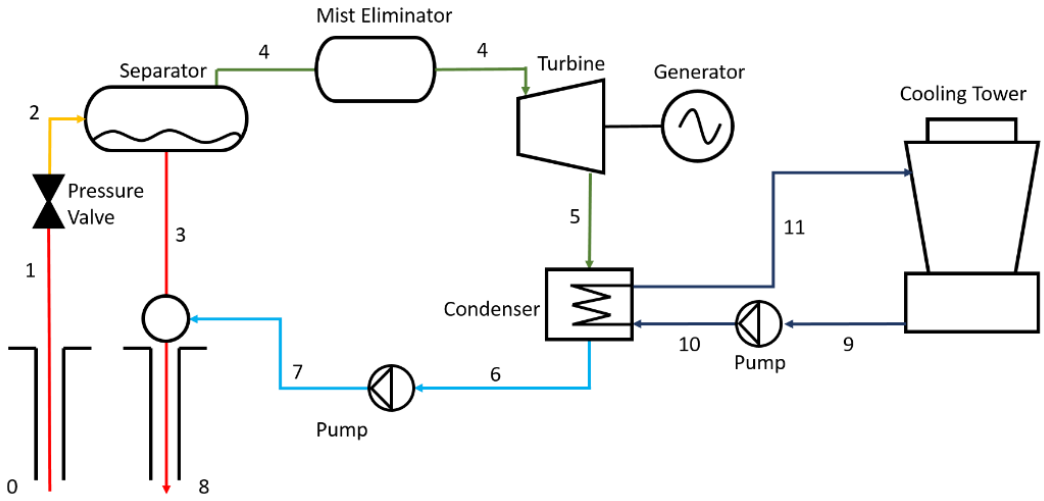

Figure 2.1: Schematic of a single-flash geothermal power plant. The red lines represent brine, yellow two-phase fluid, green steam, light blue condensate and dark blue cooling water

Table 2.1: List of components in a single-flash plant, excluding the gathering system (DiPippo, 2012)

Components	**Location, Figure 2.1**	**Description**
Mist Eliminator	4-4	Removing unwanted droplets of water in steam with efficiency of up to 99.9%
Safety Valves	Not illustrated	For safety and control. Located between mist eliminator and turbine
Turbine	4-5	Expanding and utilizing kinetic energy of working fluid to generate electrical power
Condenser	5-6 & 10-11	Tube and shell heat exchanger, steam condenses as cooling water heats up
Pump	6-7 & 9-10	Increases pressure of a certain type of liquid at a certain location
Cooling Tower	11-9	Cooling water is cooled down with air by evaporative cooling, cooling water reused
Reinjection Well	8	Reinjection into the reservoir, important for sustainable utilization of resource

Flash steam power plants are built on the flashing process of a single- or two-phase fluid. A flashing process is when the fluid is led through a pressure valve, decreasing the pressure of the fluid. If the fluid was single-phase liquid before the flashing process, the pressure is decreased below the saturation pressure for the temperature of the fluid, turning the fluid into a mixture of liquid and vapor. If the fluid was already two-phase, which is the most common case in Iceland (Pálmason, 2005), the steam fraction of the fluid increases with

decreasing pressure. After being flashed, the fluid goes through a separator, separating the liquid part from the steam. While the steam is utilized for electrical power production, the separated brine is either reinjected back into the reservoir or utilized further by heating up another fluid or even separated again. Flash steam systems are categorized by how many times the fluid coming from the gathering system is flashed and separated; single-flash, double-flash and triple-flash (DiPippo, 2012).

2.1.2 Binary Cycle System

Binary cycles utilize heat from a fluid to warm up a working fluid within an enclosed loop. When utilizing geothermal energy with a binary cycle, brine is preferred as the hot fluid because steam could already be utilized for power generation. The brine is led through heat exchangers where it heats up a working. The working fluid boils and is even superheated before it is led through an expander, generating electrical power. The state of the working fluid after expansion depends on the fluid properties and the slope of its saturation curve. After being expanded, the working fluid is cooled down to saturated liquid and increased in pressure before being heated up again (Dickson & Fanelli, 2013).

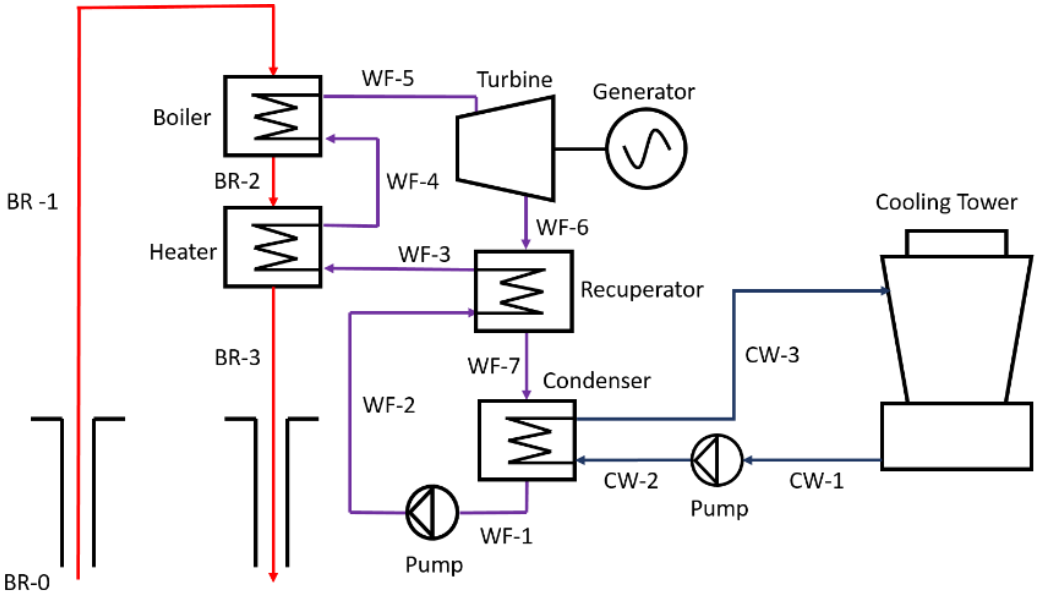

Figure 2.2: Schematic of an ORC geothermal power plant. Red lines represent brine, purple working fluid and dark blue cooling water. BR stands for brine, WF working fluid and CW cooling water

Organic Rankine cycles have been used as standalone systems or as bottoming units in geothermal application (Taylor et al., 2014). With the setup of each plant rather similar, the main difference between geothermal ORC plants is the choice of working fluid. That choice is highly dependent on the properties of both the heat source and the working fluid. Many studies have been carried out on the choice of working fluids for ORC application (Taylor et al., 2014) (Bao & Zhao, 2013). When choosing a working fluid for an ORC system, the rule-of-thumb is to choose the one which has most similar critical temperature as the high temperature of the heat source (Valdimarsson, 2016). The most common working fluids are hydrocarbons, e.g. Butane and Pentane, and refrigerants, such as hydrofluorocarbons (HFCs). Hydrocarbons have the drawback of being highly flammable while refrigerants, being non-flammable, have higher global warming potential (Taylor et al., 2014).

Table 2.2: List of components in a binary power plant, excluding the gathering system (DiPippo, 2012)

Components	Location, Figure 2.2	Description
Heater	WF-3 – WF-4 BR-2 – BR-3	Shell and tube heat exchanger, utilizing heat from the brine to heat up the working fluid
Boiler	WF-4 – WF-5 BR-1 – BR-2	Kettle boiler, utilizing heat from the brine to boil the working fluid, even superheat it
Turbine	WF-5 – WF-6	Expanding and utilizing kinetic energy of working fluid to generate electrical energy
Recuperator	WF-6 – WF-7, h. side WF-2 – WF-3, c. side	Shell and tube heat exchanger, using hotter working fluid to heat up a colder side
Condenser	WF-7 – WF-1 CW-2 – CW-3	Tube and shell heat exchanger, working fluid condenses as cooling water heats up
Pump	WF-1 – WF-2 CW-1 – CW-2	Increases pressure of a certain liquid type at a certain location
Cooling Tower	CW-3 – CW-4	Cooling water is cooled down with air by evaporative cooling, cooling water reused

2.1.3 Combined System

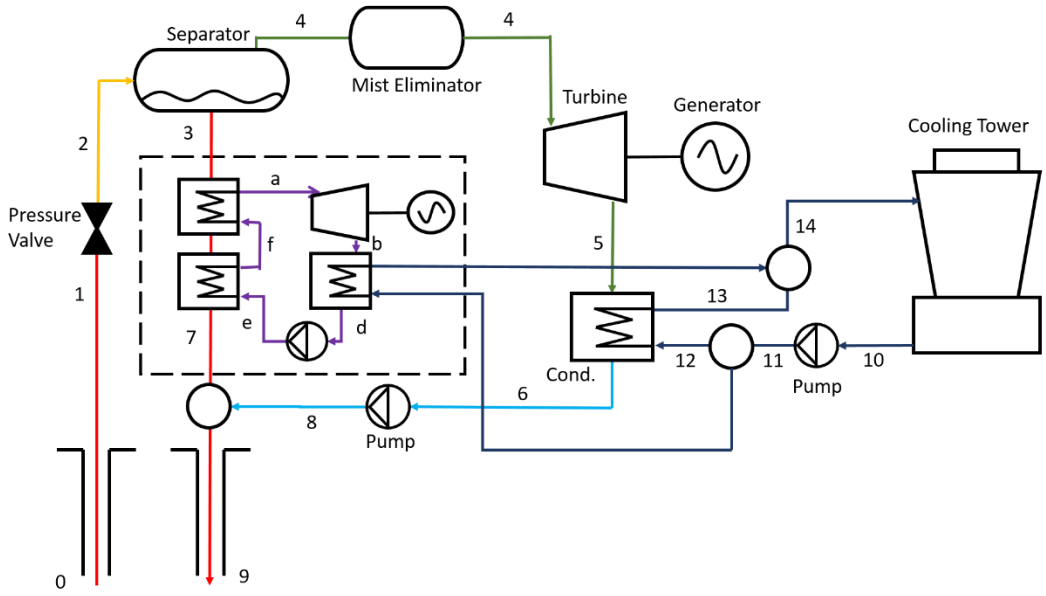

Figure 2.3: Schematic of a hybrid system, a single-flash steam cycle and a binary cycle with the latter located within the black dotted box. Red lines represent brine, yellow two-phase fluid, green steam, purple working fluid, light blue condensate and dark blue cooling water

Geothermal power plants utilize resources in many different ways. Some resources demand more sophisticated energy conversion systems than the basic ones considered above. Integration of different types of power plants are often needed to fit the needs of specific geothermal fields. Common hybrid systems in geothermal utilization are combined flash systems, flash system and a binary system and combined heat and power (CHP) systems. The benefit of integration is higher overall efficiency. On the other hand, integration leads to more difficulties with utilization, e.g. increased effects of scaling and corrosion in surface equipment. These problems are solvable and have to be considered before constructing a hybrid system (DiPippo, 2012). The focus of this study was utilizing seasonal surplus heat from geothermal CHP plants with a power generating bottoming unit. The bottoming units chosen were a single-flash steam cycle and an organic Rankine cycle. The problems considered when utilizing separated brine where availability, scaling and corrosion.

2.2 Nesjavellir Geothermal Plant

Nesjavellir is a single-flash CHP plant, also called a co-generation plant. It is located in Southwestern part of Iceland, 35 km West of Reykjavík, at the Southwestern tip of lake Þingvallavatn. The present generating capacity of Nesjavellir is 120 MW_e and 300 MW_{th}. Electricity is produced from the steam part of the reservoir fluid and the brine is utilized for district heat production. Exploration at Nesjavellir started 1946 whereas production of heat began in 1990 with capacity of 100 MW_{th}. Since then, capacity was increased in 1995, 1998 when electricity production began, 2001 and finally reaching current capacity in 2005 (Zarandi & Ívarsson, 2010). The heat produced at Nesjavellir is utilized in Reykjavík and surrounding municipalities while the electricity is used both for aluminum production and domestic usage (Kjartansson, 2015).

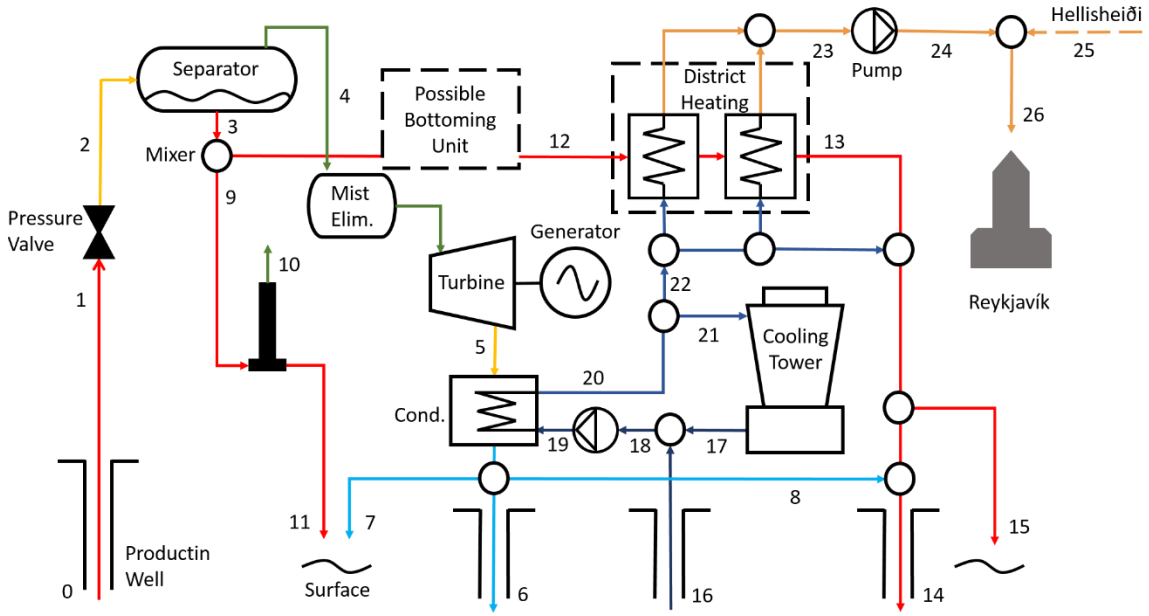

Figure 2.4: A diagram of the electricity and heat production at Nesjavellir. Red lines represent brine, yellow two-phase fluid, green steam, light blue condensate, dark blue cooling water and orange district heating water. Dashed orange line represents heat production from Hellisheiði (25)

16 production wells are currently connected through the gathering system to the power house, all of which produce 15-50 kg/s of two-phase fluid. The designed separation pressure was 14 bar_g but today it is 13 bar_g. After separation, the mass flow of brine is approximately 230 kg/s while the vapor is more than 240 kg/s. There are four 30 MW_e turbines at Nesjavellir, producing work from the steam's kinetic energy. Each unit is a condensing turbine, meaning that the pressure of the steam leaving the turbine reaches below atmospheric pressure. After the turbine, the steam is cooled down in condensers. For three of the four turbine units, the cooling water supplied to the condensers is groundwater from a shallow reservoir, 8-12°C. The fourth and most recent unit is cooled down partially with reused cooling water circulating in a cooling system. The cooling water is led through an induced draft cooling tower, cooling the water with air by evaporation (Kjartansson, 2015).

Heat produced at Nesjavellir is transported to the central district heating system in Reykjavík mainly for house heating. Approximately 68°C warmed up groundwater leaves the condensers after cooling the steam, see 20 in Figure 2.4. The heated up groundwater is warmed further up to 87°C by the 195.1°C brine coming from the separators. Before being sent to Reykjavík, the heated up groundwater is led through a deaerator, not seen in Figure 2.4 (Kjartansson, 2015). The purpose of deaeration is to remove dissolved oxygen in the water and therefore prevent or minimize corrosion in the district heating network (DiPippo, 2012). After deaeration, the heated up groundwater leaves Nesjavellir as district heating water at 84-85°C for utilization (Kjartansson, 2015).

The district heat production from Nesjavellir is interconnected to the heat production at Hellisheiði, another geothermal CHP plant located Southwest of Nesjavellir, 25 km East of Reykjavík (Júlíusson et al., 2016). The production capacity of Hellisheiði is currently 303 MW_e and 133 MW_{th} with a planned expansion in thermal production in the foreseeable future (Kjartansson, 2010). During periods of low heat demand, e.g. summer time, both geothermal CHP plants produce less than 50% of installed thermal capacity. The brine not utilized for district heat production at Nesjavellir is either reinjected or separated at atmospheric pressure and disposed of above ground, see 10 and 11 in Figure 2.4 (Kjartansson, 2015). This causes a greater environmental impact in the area and decreased overall efficiency of the plant. The idea of this study is to utilize the excess heat at Nesjavellir to produce more electricity with a bottoming unit during periods of low district heat demand.

The term seasonal surplus is a known concept in the energy industry. In this study, seasonal surplus refers to excess of thermal energy at a certain location. The seasonal excess at Nesjavellir is the thermal energy in the brine, currently utilized for district heat production. During the summer time, the lowest district heating production at Nesjavellir is currently 500-600 kg/s of 85°C hot water or approximately 40% of installed capacity (Kjartansson, 2015). This great seasonal surplus is either disposed of above ground or pumped into a shallow reservoir below the groundwater reservoir. The seasonal surplus could be utilized in an economical feasible way by generating more electrical power with a bottoming unit. The bottoming unit would produce electricity from the seasonal surplus while meeting low heat demand. The power generating bottoming unit would have to recede for increased demand of district heat.

Both Nesjavellir and Hellisheiði CHP plants fulfill the heat demand for a certain district in Reykjavík. When heat demand is low, heat produced at Hellisheiði could meet most of the demand from both CHP plants. This would result in more seasonal surplus available at Nesjavellir. With increased surplus heat at Nesjavellir, the bottoming unit in question could

theoretically produce more electrical power. The amount of electrical power is calculated with a static thermodynamic model and optimized in MATLAB®. Before the thermodynamic modelling, some calculations are done on the availability and amount of seasonal surplus at Nesjavellir. The calculations are performed with knowledge of the interconnection and a planned expansion in heat production at Hellisheiði.

Data was received from ON Power about heat production from both Nesjavellir and Hellisheiði geothermal CHP plants. The data received extended over the year 2014, with hourly resolution of district heat production being sent from each geothermal plant to Reykjavík. By interpreting the hourly heat production data as demand for district heat, the surplus of heat could be maximized at one location by producing more heat at the other location. Therefore, the hourly production data gotten from ON Power was interpreted as demand from both plants to calculate the amount of theoretical surplus at Nesjavellir. A model was setup to calculate a new set of data. The calculated data met the interpreted hourly demand in Reykjavík while maximizing surplus at Nesjavellir.

The output of the model was available thermal energy at Nesjavellir throughout the span of one year. The heat available is in the separated brine and could be utilized further in a power generating bottoming cycle with certain limitations. Four different scenarios of heat demand were calculated, present and three other future scenarios. According to researchers at ON Power, the yearly increase in heat demand is 1.5%, evenly distributed throughout the year. The surplus heat at Nesjavellir was maximized for all demand scenarios. The present scenario used original data as demand. The future scenarios were calculated demand in 2020 and 2030 without expansion at Hellisheiði and the last scenario with demand in 2030 with the expansion in heat production at Hellisheiði.

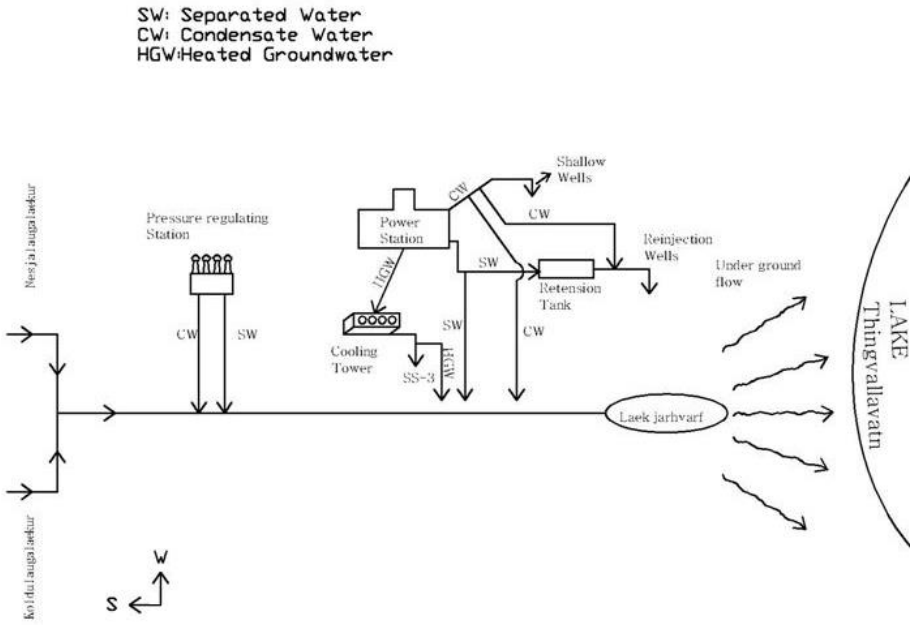

Figure 2.5: Diagram of waste flows in and out of Nesjavellir CHP plant (Zarandi & Ívarsson, 2010)

The surface and groundwater around Nesjavellir are affected by thermal pollution due to current surface disposal of waste brine. According to Zarandi & Ívarsson (2010), hot waste brine is released close to Nesjavellir power plant either into man-made wells or into the

natural runoff. It flows by gravity north, towards lake Þingvallavatn. In general, the whole area north of Nesjavellir has experienced an increase in temperature since measurements began in 2000. With utilization of this surplus heat, the amount of disposed waste brine should decrease and in all likelihood the environmental impact from the power plant would reduce.

Changes in setup at Nesjavellir cause changes in environmental impact. A slight increase in gas emissions is expected from a single-flash bottoming cycle but no changes would be expected from a binary cycle (DiPippo, 2012). The greater concern for a binary cycle would be the choice of working fluid. Different precautions must be taken with different working fluids. Hydrocarbons used in ORCs are flammable and pose an increased explosion risk. Refrigerants, which typically are not flammable, can have greater environmental risks and some refrigerants have a high ozone depletion and global warming potential (Taylor et al., 2014). The location of the bottoming cycle would be within the Nesjavellir area and therefore no new land for industrial usage would be need for the expanded utilization.

Both corrosion and scaling are expected in geothermal application. Corrosion is defined as the natural process of deterioration of metals and alloys in a corrosive environment. The most common form is uniform corrosion with other types of localized corrosions being dominant in different locations. A fluid can be corrosive at one point but changing to passive and even leaning towards scaling at another due to change in physical and chemical parameters. Scaling is precipitation of minerals former dissolved in the fluid. Although corrosion and scaling can occur during utilization of geothermal resources, it should not be a limiting factor. Both can be avoided or minimized with material selection, engineering and proper control methods (Karlsdóttir, 2012).

Table 2.3: Fluid properties of the separated brine at Nesjavellir CHP plant, separation pressure at 13 bar_g (Gunnarsson, 2012)

Location	**Temp. [°C]**	**Fluid Descrip.**	**pH**	**Concentration of key species in fluid (mg/kg)**					
				Cl^-	CO_2	H_2S	SiO_2	SO_4^{2-}	Na
After separator	195.1	Separated brine	8.56	127.5	15.23	84	763.6	10.82	158.8

The separated fluid is not acidic but it has as relatively high concentration of dissolved chloride ions, a slightly lower concentration of hydrogen sulfide and even lower of carbon dioxide. All of the mentioned species promote a favorable environment for uniform corrosion. The pressure vessels and heat exchanger in contact with the fluid would have to consist of stainless steel. By choosing a specific type of stainless steel, e.g. austenitic (S316L) or standard duplex steel (S32205), the corrosion would be minimized and even prevented (Karlsdóttir, 2012). The material selected for the specific equipment in contact with the separated brine was standard duplex (S32205) (Tassew, 2010).

The type of scales that form due to cooling of the separated brine are precipitated amorphous silica. For evaporative cooling, during the separation process, precipitation would start at 164°C. With cooling through conductive heat exchange, the scales would start forming at 162°C (Gunnarsson, 2012). At Nesjavellir, the district heating water is warmed up with the

separated brine being cooled down to 80-90°C (Kjartansson, 2015). That causes precipitation of silica scales dissolved in the brine before cooling, going from 763.6 to roughly 500 mg(SiO_2)/kg(brine).

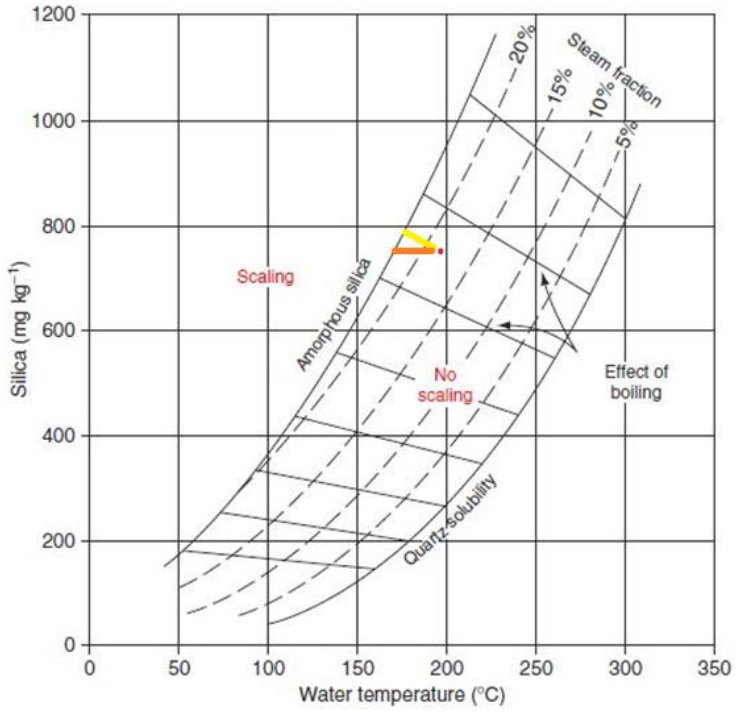

Figure 2.6: Solubility of silica in water, showing that scaling occurs above the amorphous silica solubility curve (Karlsdóttir, 2012). The red dot indicates the solubility of silica in the separated brine at Nesjavellir. The yellow lines represent cooling due to separation and the orange line cooling with heat exchanged. The temperatures when silica starts to precipitate are 164°C for evaporation (yellow) and 162°C for cooling (orange) (Gunnarsson, 2012)

Due to the fact that silica scales have a slow precipitation rate, most of the scales form after the district heat exchangers. In January 2004, a retention tank was installed in the production line at Nesjavellir, see Figure 2.5. The purpose was to give silica scales time to polymerize before reinjection. The brine leaving of the retention tank has about 500 ppm of dissolved silica. Before being reinjected, the brine is mixed with condensate to decrease the concentration of dissolved silica below 400 ppm, see 8 and 14 in Figure 2.4. This is done to prevent scaling in reinjection wells (Zarandi & Ívarsson, 2010).

For the ORC bottoming unit, the brine would go through two heat exchangers and cooled down to 90-160°C, depending on the ORC setup. The amount of silica scales can be minimized by having a forced flow of brine through the heat exchangers, causing most of the scales to precipitate later on. For the LPT bottoming unit, the brine is led through a throttling valve and then a horizontal separation tank. Scales will be prevalent in the LPT separator and possibly in the turbine. The amount of scales that precipitate depends on the lower separation pressure and time the low pressure brine spends in the separator. Silica formation in both bottoming cycles are expected to be cleaned, as is done to current heat exchangers utilized for district heat production at Nesjavellir.

3 Thermodynamic Modeling and Economic Analysis

Thermodynamic models of a low pressure flash steam cycle and an organic Rankine cycle are simulated and optimized in MATLAB®. All thermodynamic properties calculated in this study are done using CoolProp. CoolProp is an open-source database of fluid and humid air properties, formulated based on the most accurate formulations in open literature. It has been validated against the most accurate data available from the relevant references (Bell et al., 2014). Different components within the two bottoming cycles were included within each thermodynamic model. The components in question for this study are a separator, different types of heat exchangers, a pressure valve, pumps, fans, expanders and cooling towers.

The input of thermal energy comes from the separated brine. For the flash steam cycle, the brine is separated at a lower pressure, the steam part utilized for power production and low pressure brine for district heat production. For the organic Rankine cycle, either the total brine mass flow rate is led through the ORC heat exchangers and then utilized for district heat production or the mass flow is split up, with a portion going to the ORC unit and rest used for the district heat production. The cost of the equipment in each cycle is estimated using data and cost equations. The total capital and operational expenditure are assumed from the purchased equipment cost.

3.1 Thermodynamics

The properties of a fluid are the most vital information in a thermodynamic model involving power plant calculations (DiPippo, 2012). The most relative properties for this study were pressure p [Pa or bar], temperature T [°C or K], specific enthalpy h [J/kg], specific entropy s [J/(kg K)], specific volume υ [m^3/kg] and mass fraction x [-]. Two properties are needed to calculate most other properties. The mass fraction is useful when dealing with two-phase fluid. The thermodynamic processes denote changes in fluid properties. It depends on the fluid inlet properties, on the component type and fluid outlet properties. The four basic processes are an isentropic process with specific entropy being constant over a process, an isenthalpic process with specific enthalpy being constant over a process, an isobaric process with pressure being constant through a process and a heat transfer process with temperature playing a vital part in the process.

For the thermodynamic processes to be steady state, the mass flow in and out of each component must be in balance. The balancing equations are named the mass balance equation and the energy balance equation. For a component with two inputs (1 and 2) and two outputs (3 and 4), the mass balance would state:

$$\dot{m}_1 + \dot{m}_2 = \dot{m}_3 + \dot{m}_4 \tag{3.1}$$

Where $\dot{m}$ is mass flow rate in kg/s. Similar to the mass balance equation, the energy balance equation is fulfilled when the total energy flowing into a component is equal to the energy flowing out of it. Flow of energy has three main forms; energy content of the fluid $\dot{m}h$, work performed or consumed by the component $\dot{W}$ and heat flowing into or out of the component $\dot{Q}$. For a case with one inlet (1), one work input (2), one outlet (3) and one heat outflow (4), the energy balance states:

$$\dot{m}_1 h_1 + \dot{W}_2 = \dot{m}_3 h_3 + \dot{Q}_4 \tag{3.2}$$

For a steady process, both energy and mass balance equations must be fulfilled. These equations were governing in the static thermodynamic models.

3.2 Energy and Exergy

Energy analysis of a power cycle or a power plant is usually based on the conservation principle of the first law of thermodynamics. For energy analysis, an equation is used to quantify the energy efficiency of a specific thermodynamic cycle. The equation is the ratio of total work output to total heat input and is called the first law efficiency, or thermal efficiency:

$$\eta_{th} = \eta_I = \frac{\text{Net Work Output}}{\text{Total Heat Input}} = \frac{\dot{W}_{net}}{\dot{Q}_{in}} \tag{3.3}$$

Another useful term in thermodynamic modelling is exergy, used in exergy analysis. The useful energy, or exergy, of a stream is stated as:

$$e = (h - h_0) - T_0(s - s_0) \tag{3.4}$$

The subscript 0 represents properties for the "dead state" or the environment. By introducing the mass flow of the stream, the exergy flow rate is obtained:

$$\dot{E} = \dot{m}e \tag{3.5}$$

The exergy efficiency, also known as second law efficiency, is used to quantify the utilization efficiency of a specific thermodynamic cycle (DiPippo, 2012). It gives a much better indication of the design quality of a power plant than the thermal efficiency and is defined as:

$$\eta_{II} = \frac{\text{Net Work Output}}{\text{Total Exergy Input}} = \frac{\dot{W}_{net}}{\dot{E}_{in}} \tag{3.6}$$

3.3 Organic Rankine Cycle (ORC)

The organic Rankine cycle was chosen as a power generating bottoming cycle, utilizing seasonal surplus from Nesjavellir. The seasonal surplus heat is utilized by heat transfer, cooling the brine while heating up a working fluid. The brine leaves the separator as saturated liquid at 13 bar_g, at 195.1°C. The brine warms up and boils a working fluid until it is saturated steam. No superheating or trans-critical heating was taken into consideration in the ORC thermodynamic model. After reviewing theory on working fluids for ORCs, six different working fluids were chosen for this study, see 4.1. Two different kinds of setup were taken into consideration for the ORC, a serial setup and a parallel setup.

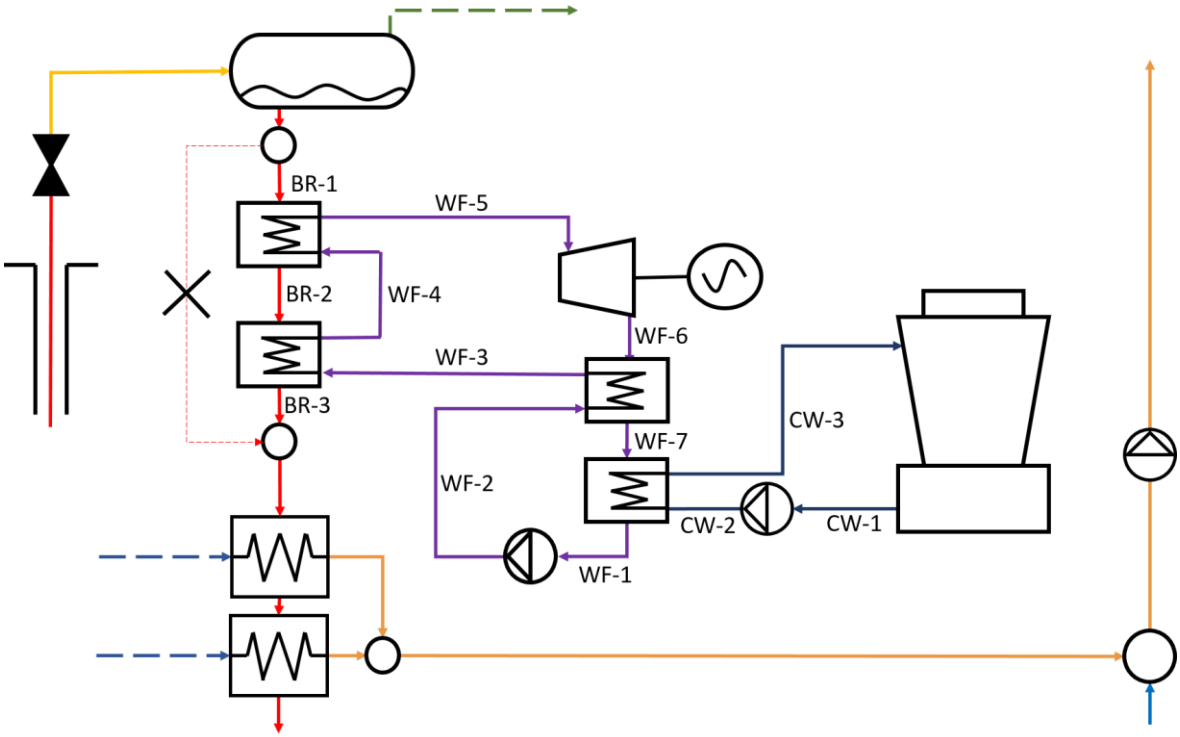

Figure 3.1: Schematic of an ORC and a possible set up at Nesjavellir (serial setup). Red lines represent brine, yellow two-phase fluid, dotted green line steam going to main turbines, purple lines the working fluid, light blue dotted lines the heated up cold water from current condensers, orange district heating water and dark blue cooling water. BR stands for brine, WF for working fluid and CW cooling water

There are only two pressure levels of the working fluid due to the assumption that no pressure losses are prevalent in the system. The working fluid, coming out of the condenser at low pressure as saturated liquid, goes through the working fluid pump (WF1-WF2) and increase to the high pressure level. It travels through the heat exchangers, recuperator (WF2-WF3), heater (WF3-WF4) and boiler (WF4-WF5), at high pressure. It enters the expander (WF5-WF6) as saturated vapor and decreases in pressure as it flows through, producing work from thermal energy in the working fluid. After the expander, the low pressure working fluid is cooled down in the recuperator (WF6-WF7) before being condensed to saturated liquid in the condenser (WF7-WF1).

The brine is cooled down in the heat exchangers, boiler (BR1-BR2) and heater (BR2-BR3). Thermal energy travels with conductive heat transfer from the brine to the working fluid in the heat exchangers. The assumption was made that no heat was lost to the environment

during the isobaric heat transfer processes. The circulating cooling water goes through the cold water pump (CW1-CW2) and increases in pressure before being heated up in the condenser (CW2-CW3). The warmer cooling water enters the wet cooling tower and is cooled down by evaporation. The cooling tower has a fan stacked at the top which causes an induced draft of air travelling up and through the cooling tower, cooling the water.

Table 3.1: Components in the ORC setup at Nesjavellir

Component	**Location, Figure 3.1**	**Description**
Pump	WF1 – WF2 CW1 – CW2	Fluid enters at a lower pressure and leaves at higher pressure. Entropy is created in the pumping process, fluid leaves slightly warmer
Recuperator (T&S)	WF2 – WF3 (Cold) WF6 – WF7 (Hot)	Fixed head. Working fluid leaving the turbine heats up the colder fluid at higher pressure. Isobaric internal heat recovery, no heat loss
Heater (T&S)	WF3 – WF4 BR2 – BR3	Floating head. The brine heats up the high pressure working fluid to saturated liquid. Isobaric heat exchanging, no heat loss
Boiler (T&S)	WF4 – WF5 BR1 – BR2	Kettle boiler heat exchanger. The brine boils the high pressure working fluid to saturated vapor. Isobaric heat exchanging, no heat loss
Turbine	WF5 –WF6	Working fluid (saturated vapor) decreases in pressure while kinetic energy from the fluid is transformed to work. Entropy is created
Condenser (T&S)	WF6 – WF7 CW2-CW3	U-tube heat exchanger. Condensation takes place as the cooling water heats up. Isobaric heat exchanging, no heat loss
Cooling Tower	CW3 – CW1 CA1 – CA2 (not seen)	Cooling water undergoes evaporative cooling. Air coming into the tower leaves the cooling tower with 95% relative humidity

All the following equations and theory on thermodynamic processes were gotten from two sources, DiPippo (2012) and Dickson & Fanelli (2013). The working fluid coming out of the condenser as saturated liquid at low pressure, increases in pressure due to work done by the pump. For an isentropic pumping process, the entropy would be the same before and after. The pumping process is assumed non isentropic, instead the isentropic efficiency of the pump is defined:

$$\eta_{is,pu} = \frac{h_{2is,wf} - h_{1,wf}}{h_{2,wf} - h_{1,wf}} \tag{3.7}$$

By assuming the isentropic efficiency of the pump and calculating the real enthalpy after the pump, the work done by the pump can be derived:

$$\dot{W}_{pu} = \dot{m}_{wf}(h_{2,wf} - h_{1,wf}) \tag{3.8}$$

After the pump, the high pressure working fluid, cold side, flows through the recuperator, exchanging heat with the low pressure working fluid coming out of the turbine, hot side. The heat exchanging process is isobaric. The energy balance over the recuperator is:

$$\dot{m}_{wf}\left(h_{3,wf} - h_{2,wf}\right) = \dot{m}_{wf}(h_{6,wf} - h_{7,wf}) \tag{3.9}$$

Different working fluids were chosen for optimization. The working fluids chosen are described as dry, isentropic or wet fluids. This description depends on the behavior of the vapor saturation curve for each fluid. For dry fluids, the vapor saturation curve in a T-s diagram has a positive slope at most parts. For the isentropic fluids, the slope is relatively vertical. For the wet fluids, the slope is negative at most parts. A constraint was given for the recuperator. When not enough heat was available in the hot side of the working fluid, the recuperator would be taken out of the system, meaning no internal heat recovery. That was the case for the isentropic and wet working fluids, more information in 4.1 below. The total thermal energy entering the system comes from the seasonal surplus, the brine:

$$\dot{Q}_{in} = \dot{Q}_{bo} + \dot{Q}_{he} = \dot{m}_{br}\left(h_{1,br} - h_{3,br}\right) \tag{3.10}$$

The heat transfer in the heater and boiler are assumed isobaric for both fluids and no heat is lost to the environment. The heat transfer in the heater is stated with an energy balance:

$$\dot{m}_{br}(h_{2,br} - h_{3,br}) = \dot{m}_{wf}(h_{4,wf} - h_{3,wf}) \tag{3.11}$$

The working fluid leaves the heater as saturated liquid. After the heater, the working fluid flows through and evaporates in the boiler. The energy balance over the boiler is:

$$\dot{m}_{br}(h_{1,br} - h_{2,br}) = \dot{m}_{wf}(h_{5,wf} - h_{4,wf}) \tag{3.12}$$

The working fluid leaves the boiler as saturated vapor. Neither superheating nor trans-critical heating were assumed in these thermodynamic calculations. Superheating refers to that the working fluid is superheated after becoming saturated vapor. Trans-critical heating refers to heating at a pressure level above the critical point of the fluid, from subcooled state directly to superheated state.

The working fluid enters the turbine at a high pressure level, decreasing in pressure and transforming kinetic energy to work. The expanding process in the turbine is assumed non isentropic. The isentropic efficiency of the turbine is:

$$\eta_{is,turb} = \frac{h_{5,wf} - h_{6,wf}}{h_{5is,wf} - h_{6,wf}} \tag{3.13}$$

The work performed by the turbine is calculated as:

$$\dot{W}_{turb} = \dot{m}_{wf}(h_{5,wf} - h_{6,wf}) \tag{3.14}$$

Afterwards, the working fluid is cooled further by exchanging heat with the recirculating cooling water. The working fluid condenses as the cooling water increases in temperature. The heat exchanging process in the condenser is assumed isobaric and the energy balance through it is:

$$\dot{m}_{br}(h_{7,br} - h_{1,br}) = \dot{m}_{cw}(h_{3,cw} - h_{2,cw}) \tag{3.15}$$

The following equations and theory on wet cooling towers were gotten from two sources, Papaefthimiou et al. (2006) and Pálsson (2014). The design criteria for the cooling tower was to make it similar to operating cooling towers at Nesjavellir. The induced draft fan at the top of the cooling tower forces the air coming to the cooling tower at the sides (CA1), through the fill and up through the cooling tower (CA2), see Figure 3.2. Due to the evaporation of water in the cooling process, some amount of water must be added to the cooling tower as make-up water to maintain proper function of the cooling process.

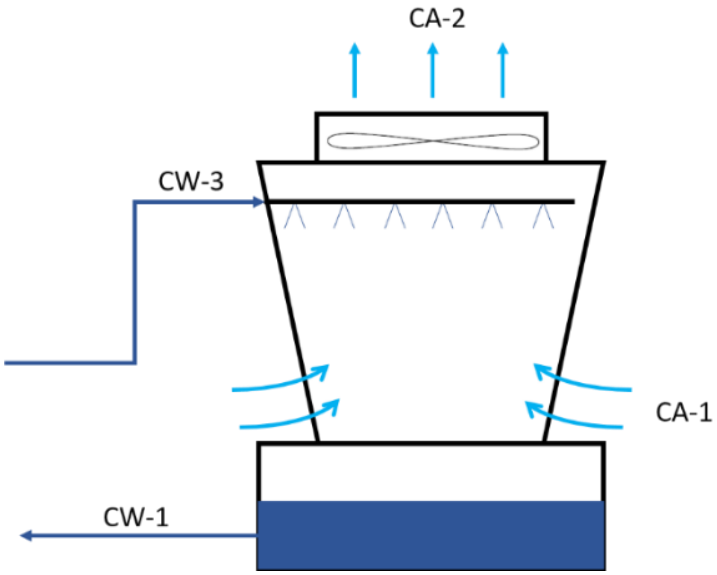

Figure 3.2: Process diagram of the wet cooling tower. CW stands for cooling water and CA cooling air

Air coming in at CA1 has less water particles in it than the air going out at CA2. Relative humidity is a term used for concentration of water particles with in air. Relative humidity is the ratio between partial pressure of water within the air and the saturation pressure of water at the temperature of the air:

$$\phi = \frac{p_w}{p_s} \tag{3.16}$$

For a sufficiently large cooling tower, it can be assumed that the air leaving at CA1 is at 100% relative humidity. For this study, 95% was assumed at the outlet. For the inlet, data was gotten from the Icelandic Meteorological Office (IMO) and was assumed 65% average relative humidity at Nesjavellir. Another term called humidity ratio is expressed as the ratio between the actual mass of water vapor present in moist air and the mass of the dry air:

$$\omega = \frac{x_w}{x_a} = \frac{M_w\, \phi p_s}{M_a(p - \phi p_s)} \tag{3.17}$$

Where M is molar mass [kg/mol] and subscripts a, w and s stand for air, water and saturation respectively. The cooling process in the cooling tower is assumed as stead state. For a steady process, both energy and mass balance equations must be fulfilled. Mass balance in the cooling tower for water and air are stated as:

$$\dot{m}_{3,cw} + \dot{m}_{1,ca,w} = \dot{m}_{1,cw} + \dot{m}_{2,ca,w} \tag{3.18}$$

$$\dot{m}_{1,ca,a} = \dot{m}_{2,ca,a} = \dot{m}_a \tag{3.19}$$

The energy balance of the process is stated as:

$$\dot{m}_{3,cw}h_{3,cw} + \dot{m}_{1,ca,w}h_{1,ca,w} + \dot{m}_a h_{1,ca,a} = \dot{m}_{1,cw}h_{1,cw} + \dot{m}_{2,ca,w}h_{2,ca,w} + \dot{m}_a h_{2,ca,a} \tag{3.20}$$

By knowing the relative humidity and being able to calculate the humidity ratio, the mass flow rate of water coming in at CA1 can be written differently, $\dot{m}_{1,ca,w} = \omega_{1,ca}\dot{m}_a$. Same goes for the water going out at CA2, $\dot{m}_{2,ca,w} = \omega_{2,ca}\dot{m}_a$. The mass blance of water is then:

$$\dot{m}_{3,cw} = \dot{m}_{1,cw} + (\omega_{2,ca} - \omega_{1,ca})\dot{m}_a \tag{3.21}$$

By rearranging the energy balance equation, the mass flow rate of air and the make-up water needed to maintain full function of the cooling tower are calculated. The work performed by the induced draft fan at the top of the cooling tower is calculated by:

$$\dot{W}_{fan} = \dot{m}_a \frac{p_{2,ca} - p_{1,ca}}{\rho_{2,ca}} \tag{3.22}$$

Where the difference in pressure between CA1 and CA2 is the difference in total pressure in both locations. By assuming the static pressure is the same, the term becomes the difference in dynamic pressure. The dynamic pressure was calculated by assuming the diameter of the fan as 6m, and calculating the velocity of air going out of two cooling water cells.

The isentropic efficiency of the cooling water pump and work needed for the process are similar to Equations (3.7) and (3.8) above. The electrical power generated or consumed by components was calculated by assuming mechanical efficiency.

There were two different kinds of setups considered for the ORC bottoming unit, a serial setup and a parallel setup. The main difference between the setups is the mass flow of the brine. For the serial setup, all of the mass flow of separated brine is led through the heat exchangers. The brine is cooled down to a level of 130-150°C and the rest of the brine utilized to fulfill the district heat demand from Nesjavellir. When demand for district heat increases due to colder weather, the ORC would be shut down and the mass flow of brine is led straight through the district heat exchangers, see Figure 3.3a.

For the parallel setup, the mass flow of separated brine is split up. Part of the mass flow goes to the ORC and the other part to the district heat exchangers. Although lower mass flow rate going to the ORC, the same amount of heat is utilized to heat up and boil the working fluid. The brine being led through the ORC is cooled further down than in the serial setup, down to 80-100°C, and not utilized for heat production afterwards. The cold brine coming from the parallel ORC setup is sent to the retention tank before being either reinjected or disposed

of above ground. Similar for the serial setup, when heat demand increases, the total mass flow of brine is utilized for district heat production, see Figure 3.4a.

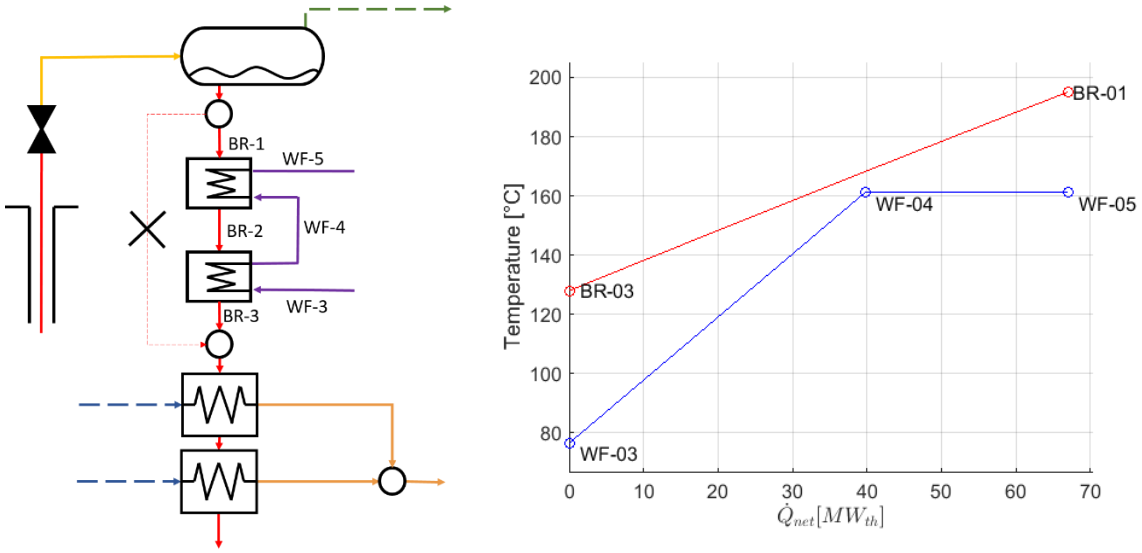

Figure 3.3a (left): ORC serial setup. 3.3b (right:) T-Q diagram of heater and boiler for ORC serial setup

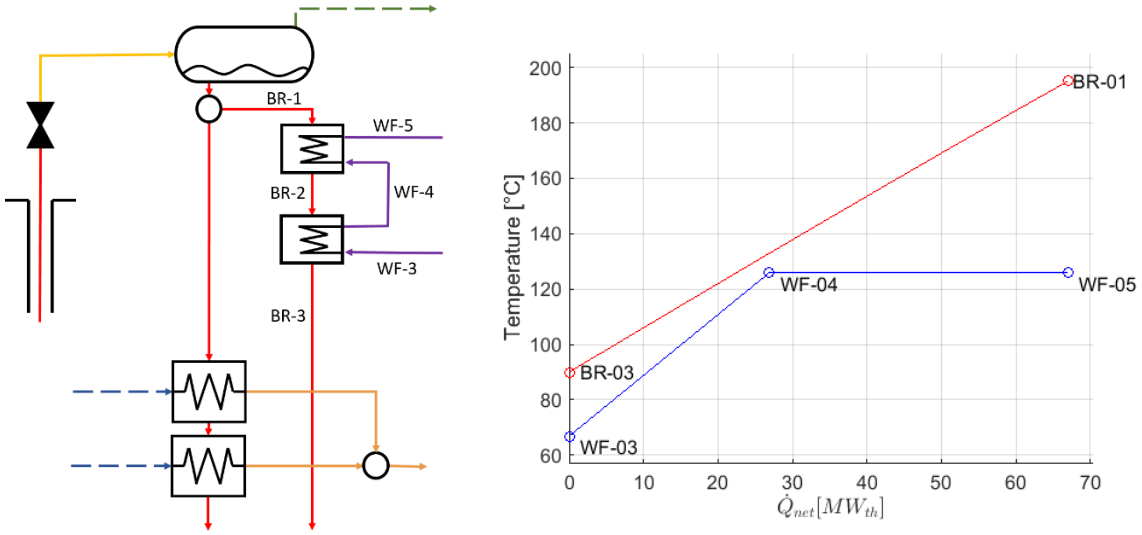

Figure 3.4a (left): ORC parallel setup. 3.4b (right): T-Q diagram of heater and boiler for ORC parallel setup

3.4 Low Pressure Turbine (LPT) Cycle

The single-flash steam cycle was also chosen as a power generating bottoming cycle, utilizing seasonal surplus from Nesjavellir. The seasonal surplus heat is utilized by decreasing the pressure of the 13 bar_g brine and separating vapor from the liquid part. The vapor is led through an expander, generating electrical energy, while the liquid is utilized for heat production. By decreasing the pressure of the brine to 3-6 bar_a, the liquid part of the two-phase fluid should suffice the low district heat demand.

During low heat demand, the separated brine is led through a throttling valve (1-2). There the fluid undergoes a flashing process, making it a mixture of vapor and liquid. At the lower pressure level, the vapor part is separated from the liquid part (2-4 and 2-3). While the liquid part is utilized for district heat production, the vapor is expanded through a turbine (4-5). During the expansion, the vapor produces work which is turned into electrical power in the generator. The two-phase fluid coming from the expander is condensed to saturated liquid (5-6) and either reinjected or utilized further e.g. as make-up water. The high pressure cooling water used in the tube and shell heat exchanger is heated up during condensation of the two-phase fluid (8-9). It is cooled down in a wet cooling tower (9-7) and decreases in pressure. Before being reused in the condenser, the cooling water undergoes a pumping process to increase in pressure again (7-8).

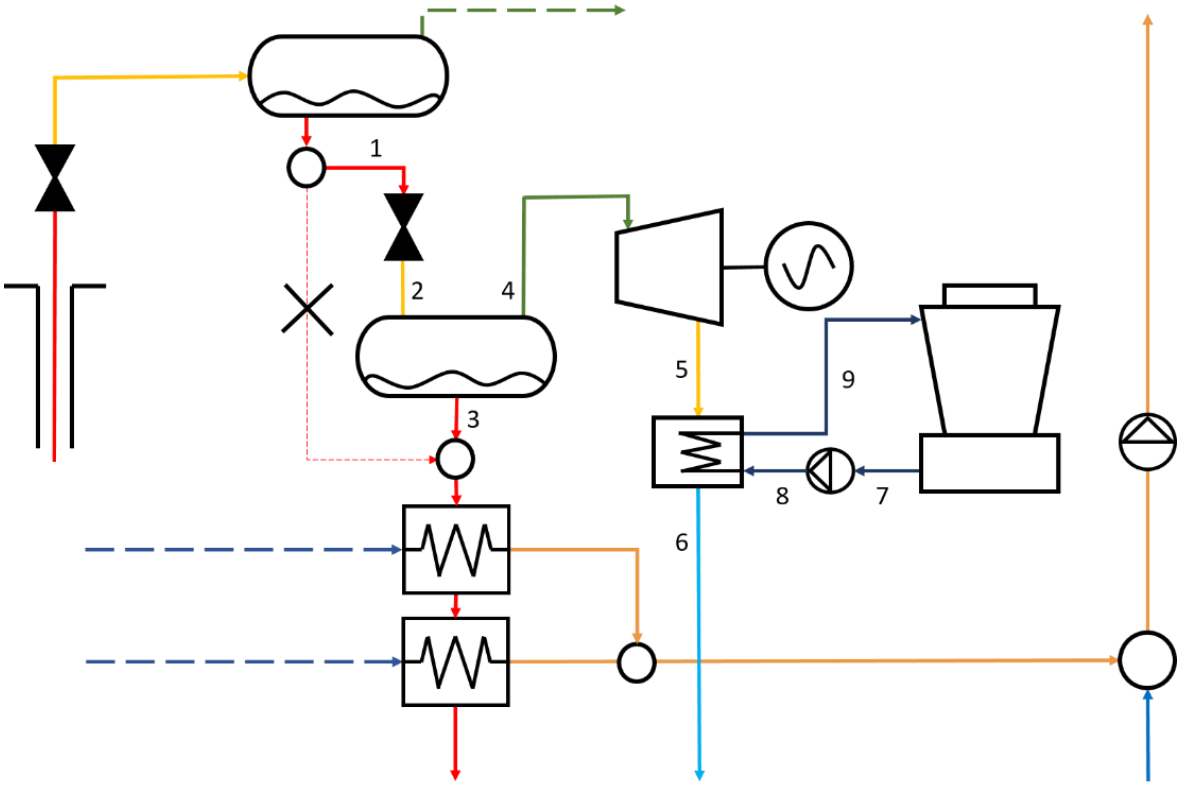

Figure 3.5: Schematic of a LPT cycle and a possible set up at Nesjavellir. Red line represents geothermal brine, yellow two-phase fluid, dotted green line steam going to main turbines, the green line the separated vapor at low pressure, light blue low pressure condensate, blue dotted lines the heated up cold water from main turbines, orange district heating water and dark blue cooling water.

Table 3.2: Components in the LPT setup at Nesjavellir

Component	Location, Figure 3.5	Description
Throttling Valve	1-2	Fluid enters at a lower pressure and leaves at higher pressure. Entropy is created in the pumping process, fluid leaves slightly warmer
Separator (Horizontal)	2-3 (Liquid) 2-4 (Vapor)	Two-phase fluid enters and is separated. Liquid used for heat production and vapor electricity production. Isobaric process, no heat loss
Turbine	4-5	Saturated vapor decreases in pressure while kinetic energy from the fluid is transformed to work. Entropy is created
Condenser (T&S)	5-6 8-9	U-tube heat exchanger. Condensation takes place as the cooling water heats up. Isobaric heat exchanging, no heat loss
Cooling Tower	9-7 CA1-CA2 (not seen)	Cooling water undergoes evaporative cooling. Air coming into the tower leaves the cooling tower with 95% relative humidity
Pump	7-8	Fluid enters at a lower pressure and leaves at higher pressure. Entropy is created in the pumping process, fluid leaves slightly warmer

All the following equations and theory on thermodynamic processes were gotten from two sources, DiPippo (2012) and Dickson & Fanelli (2013). The flashing process takes place in the throttling valve. The process is assumed isenthalpic and steady state. The energy balance over the throttling valve is stated as:

$$\dot{m}_1 h_1 = h_2 \dot{m}_2 \tag{3.23}$$

The separation is assumed an isobaric process and steady state. The energy and mass balances over the separation process are:

$$\dot{m}_2 h_2 = (\dot{m}_3 + \dot{m}_4) h_2 = \dot{m}_3 h_3 + \dot{m}_4 h_4 \tag{3.24}$$

Other thermodynamic processes are comparable to ones described for the ORC above, see Equations (3.7)-(3.22), with one addition to the efficiency of the turbine (4-5). A known rule for turbines is named the Baumann rule. It states that the turbine efficiency decreases in direct relationship with higher moisture content of the steam (DiPippo, 2012). The real efficiency of the turbine is defined by the Baumann rule as:

$$\eta_{is,turb} = \eta_{is,base} \frac{x_4 - x_5}{2} \tag{3.25}$$

3.5 Economic Analysis

The capital and operational expenditures are estimated for both types of bottoming cycles. From the CAPEX and OPEX, the levelized cost of electricity is calculated by assuming an equity-ratio and interest rates. The price for generated electricity is then compared to the selling price of electricity at a given period of the year. Inflation was not taken into consideration. These economic calculations and feasibility studies should be taken with a certain degree of uncertainty.

The American Association of Cost Engineering (AACE) International provieds guidelines for the general principles of cost estimation and classification to asset the estimates of the project. The guidelines are titled the Cost Estimation Classification System and they map the stages and phases of asset cost estimation. Five cost estimate classes have been established and are labeled Class 1 to 5, with 5 being the lowest level of cost definition. The primiary characteristic is the level of project definition, expressed as percentage of complete definition. The secondary characteristics are methodology, expected accuracy range and more (AACE, 1997). According to the guidelines and the cost estimates used in this study, this economic feasibility study is categorized as Class 5 or 4. In theses classes, the level of project definition ranges from 0% to 15% with an relative accuracy range of 3 to 20, 1 being the best relative index. Therefore the economic analysis is a preliminary feasibility study.

3.5.1 Capital and Operational Cost

The capital expenditure (CAPEX) is the initial investment cost that is needed to build up or to start a project. For a geothermal power plant, the capital is needed for exploration, purchase of land, environmental impact and pre-feasibility studies, drilling, facilities and required equipment. The difference in CAPEX for different geothermal power plants is mainly due to required equipment for future utilization, which can be linked to the size and characteristics of the geothermal reservoir. The CAPEX is distributed throughout the project until the power plant becomes fully operational (Jóhannesson & Guðmundsson, 2015)

The CAPEX for this project mostly consist of equipment purchased, housing, engineering and installation costs. The OPEX is estimated to be 1–4 % of the CAPEX per year (Jóhannesson & Guðmundsson, 2015). Together the CAPEX and OPEX form the overall cost for the bottoming cycles.

When estimating component cost, it is important to know that the accuracy of cost substantially depends on the quality of the information available for each component. For this study, costs were estimated from literature available. Firstly, the cost of the equipment was estimated by knowing the prize and the size of a component. Then the cost of the same component of a different size was calculated. An exponential law was used which defines the product cost as an exponential function of the size of the component.

$$C_{eq} = C_{base} \cdot \left(\frac{X_{eq}}{X_{base}}\right)^{\alpha} \tag{3.26}$$

Where C_{eq} is the calculated cost of a specific equipment of a size or capacity expressed by X_{eq} and C_{base} is the known cost of the same equipment with a known size or capacity of X_{base}. The scaling exponent, α, defines the slope of the log-log line and represents a cost estimating parameter (Bejan et al., 1996). Various tables are available in the literature to define α and

give a range which can be applied for each component, usually ranging between 0.4-1.2. If information is lacking about α for a specific equipment, the six-tenth rule could be applied which gives the scaling exponent a value of 0.6 (Green & Perry, 2008).

After a discussion with an employee and a geothermal expert at Verkís, the price of a condensing low pressure turbine with a generator ranges from 250-450 US$/kW with size ranging from 30 to 10 MW_e respectively (Guðmundsson, 2016). For this study, base values for Equation (3.26) for both a low pressure condensing steam turbine and a genarator were chosen as 450 US$/kW for a 10 MW_e. The same price was assumed for the ORC turbine.

This study was done in cooperation with ON Power, the municipipality owned company responsible for operations at Hellisheið and Nesjavellir geothermal plants. Cost information about a cooling tower was gotten from ON Power. The sizing factor, X_{base}, for a wet cooling tower is the mass flow rate of cooling water. The cost of turbines and cooling towers were calculated with Equation (3.26). The α values use for this study are listed in Table 3.3 below.

Table 3.3: Equation (3.26) used to calculate cost of following components. The range of alpha values was gotten from Bejan et al. (1996), Green & Perry (2008) and Guðmundsson (2016)

Component	**Sizing**	**Literature, α**	**Chosen α**
LP Turbine	Capcity	0,75 – 0,9	0,85
ORC Turbine	Capacity	0,75 – 0,9	0,85
Cooling Tower	Mass flow rate	0,93 – 1	0,95

Without any prior knowledge of component's cost or size, the exponential equation could not be used. Instead, mathematical formulas for purchasing cost were used. They are applicable in scenarios when information is scars or when cost to prepare cost estimates is too high. Purchase costs for heat exchangers, separators, pumps, motors and cooling tower fans were calculated using correlations given by Seider et al. (2009), see Equations (I.1) – (I.13) in x. They were gotten from an American source so they are in US customary units. All of the equations give a prize according to mid-2000. A cost index was used to calculate the present cost of all components calculated with equations. The cost index used is the Chemical Engineering cost index (CE). The CE in 2000 was CE_{2000} = 394 and nowadays it is CE_{2016} = 590, making the cost of equipment 50.5% more expensive now than in 2000. The US dollar is taken as 120 ISK and the Euro as 140 ISK.

The total CAPEX [ISK] is estimated from the calculated purchased equipment cost. According to Bejan et al. (1996), the installation, engineering and construction cost can be estimated as 50-100% of the purchased equipment cost. After estimating total cost, there should be added 15-20% to that cost to account for unforseable cost (Guðmundsson, 2016). That makes the total capital expenditure as 172.5-240% of the purchased equipment cost. It is assumed that the total CAPEX would be the twice the purchased equipment cost. The OPEX [ISK/yr] was assumed low, only 2% of the purchased equipment cost because no more extra personel should be needed at Nesjavellir with an additional bottoming cycle.

3.5.2 Levelized Cost of Electricity

The levelized cost of electricity, LC, is the measure of how much electricity costs per sold energy output. It is used as a basis when comparing different methods of electricity generation or when performing feasibility studies, such as this one (Seider et al.,2009). The levelized cost is calculated from the equal-amount of money transaction, $A_{eq.,}$ which is calculated from the total CAPEX and the capital recovery factor, CRF. The A_{eq} is a way of dividing the CAPEX equally throughout the lifetime of the plant:

$$A_{eq} = CAPEX \cdot CRF = CAPEX \cdot \frac{i(1+i)^n}{(1+i)^n - 1} \tag{3.27}$$

Where i is interest rate when calculating for loan and rate of return, RoR, when calculating for equity and n is lifetime of project. The equity ratio and other assumptions are listed below. The annual revenue [ISK/yr] is needed to cover the requirements of return for the investor, the loan's downpayment and the OPEX:

$$A_{eq,revenue} = A_{eq,return} + A_{eq,loan} + A_{eq,OPEX} \tag{3.28}$$

The levelized cost of electricity [ISK/kWh$_e$] is then calculated by knowing the annual revenue [ISK/yr] and the annual power production, W_{net} [kWh$_e$/yr]:

$$LC = \frac{A_{eq,revenue}}{W_{net}} \tag{3.29}$$

Another approach would be to find out what the price of electricy is and calculate backwards to the rate of return for the investor. With a suffincintly high rate of return, the project would be economically feasible (Guðmundsson, 2016).

4 Optimization

Static thermodynamic models of a low pressure flash steam cycle and an organic Rankine cycle are simulated and optimized in MATLAB®. The optimization function used is a built-in multivariable function called fmincon. The purpose of fmincon is to find a minimum while fulfilling constraints. The user defines an objective function and initial values which are either bounded or not. The user can also define constraints which can be either linear or non-linear (MATLAB, 2014). Optimization setup for each power generating bottoming cycle and the assumptions made are described in the following section.

4.1 Organic Rankine Cycle

The performance of an ORC is mainly dependent on the heat source, the setup and choice of working fluid (DiPippo, 2012). The heat source is considered as a medium-low temperature heat source. According to Astolfi et al. (2014), Quoilin et al. (2013) and Taylor et al. (2014), the choice of working fluid for a medium-low temperature heat source would be hydrocarbons, e.g. Butane and Pentane, or refrigerants, such as hydrofluorocarbons (HFCs). Four types of hydrocarbons and two types of HFCs are considered for all ORC optimizations.

Two different types of setups are chosen, a serial setup and a parallel setup. Each setup consisted of a pump, a heater, a boiler, an expander, a condenser and a cooling cycle. A recuperator was also considered but was redundant for some working fluids. That was dependent on the energy available after expansion and the vapor saturation curve. The dry working fluids, n-Pentane and Isopentane, benefitted of a recuperator and its internal heat recovery. The wet fluid, R134a, did not have enough thermal energy after expansion and therefore no recuperator is in the optimized solution. For the isentropic fluids, n-Butane, Isobutane and R245fa, the selection of a recuperator varied on the optimization.

Three different optimization modules are setup for the ORC. The input data for all three modules was the maximized seasonal surplus at Nesjavellir. Firstly, the net power output was maximized. The net energy output was maximized secondly, taking time and operational hours into consideration. Thirdly, the levelized cost of electricity was minimized, taking operating hours and economic calculations into consideration.

4.1.1 Net Power Output

The maximum value of seasonal surplus was used for net power optimization for both types of ORC setup, serial and parallel. The optimizing variables of the objective function for fmincon are the low and high pressure levels of the working fluid. The pressure levels, $P_{wf,low}$ and $P_{wf,high}$, are defined by two variables, x_1 and x_2. The defining variables for the two pressure levels are used as input variables for the fmincon objective function, x_1 optimizing $P_{wf,high}$ and x_2 optimizing $P_{wf,low}$:

$$x_1 = \frac{P_{wf,high} - P_{wf,\min}}{P_{wf,max} - P_{wf,\min}} \quad (4.1)$$

$$x_2 = \frac{P_{wf,low} - P_{wf,\min}}{P_{wf,high} - P_{wf,\min}} \quad (4.2)$$

Where $P_{wf,min}$ and $P_{wf,max}$ are the minimum and maximum pressure values of the working fluid, respectively. All of the working fluids had the same $P_{wf,min}$ = 1 kPa, but $P_{wf,max}$ was defined as 2 bar below the critical pressure of each fluid. With this definition, the input variables, x_1 and x_2, are bounded between 0 and 1. The initial values are two random numbers between 0 and 1.

Three non-linear constraints are considered. Two of the constraints are pinch point constraints, first in the heater-boiler and the second in the condenser. The objective function was formulated so that a pinch constraint was unnecessary for the recuperator. The last constraint was for the steam quality going out of the ORC expander, it was not to decrease below 85%. For a legal solution, all of the non-linear constraints had to be fulfilled.

4.1.2 Net Energy Output

The calculated data series of seasonal surplus are used for net energy optimization for both types of ORC setup. The optimizing variables of the objective function are the low pressure and high pressure levels of the working fluid and percentage of the maximum seasonal surplus. The pressure levels are formulated as seen in Equations (4.1) and (4.2). The percentage of maximum seasonal surplus was a bounded number between 0 and 1 and was defined as:

$$x_3 = \frac{\dot{Q}_{utilized}}{\dot{Q}_{available}} \quad (4.3)$$

Where $\dot{Q}$ is heat flow rate and available is the maximum value of seasonal surplus. When X_3=1, the utilized heat is the same amount of heat available while low heat demand is fulfilled. The same non-linear constraints are used for the net energy optimization as for the net power optimization. The model ran with two different scenarios for ORC turbines, either a single turbine or two turbines. The benefit of having two turbines is that when heat demand increases, one turbine could be shut down and the other kept running until heat demand increases even further. Another variable was needed for the optimization of two turbines. The fourth optimizing variable was the ratio between install capacity of one turbine and the total installed capacity:

$$x_4 = \frac{\dot{W}_{turb1}}{\dot{W}_{turb,tot}} \quad (4.4)$$

Where $\dot{W}$ is installed generating capacity and subscripts 1 and tot stand for 1 turbine and both turbines. The initial values are three and four random numbers between 0 and 1, respectively.

4.1.3 Levelized Cost of Electricity

The setup of the optimization of levelized cost of electricity was the same as for the net energy output optimization. The only difference was the added economic calculations and the output value of the objective function.

4.2 Low Pressure Turbine

The performance of a LPT cycle is dependent on the energy source and setup (DiPippo, 2012). Three different optimization modules are setup for the LPT. The optimization was the same as for the ORC, net power output, net energy output and levelized cost of electricity.

4.2.1 Net Power Output

The input variables of the objective function for fmincon are separation pressure and condensing pressure levels for the LPT setup. The pressure levels, P_{sep} and P_{cond}, are defined by two variables, x_1 and x_2. The defining variables for the two pressure levels are used as input variables for the fmincon objective function, x_1 optimizing P_{sep} and x_2 optimizing P_{cond}:

$$x_1 = \frac{P_{sep} - P_{\min}}{P_{max} - P_{\min}} \tag{4.5}$$

$$x_2 = \frac{P_{cond} - P_{\min}}{P_{sep} - P_{\min}} \tag{4.6}$$

Where P_{min} and P_{max} are the minimum and maximum pressure values of the low pressure steam, respectively. The minimum value was P_{min} = 1 kPa, and P_{max} was defined as 13 bar_g or the current separation pressure at Nesjavellir. With this definition, the input variables, x_1 and x_2, are bound between 0 and 1. The initial values are random numbers between 0-1.

Three non-linear constraints are considered. The first was that the steam quality after expansion was not to decrease below 85%. The second was a pinch point constraint in the condenser. The third was that minimum heat demand would be fulfilled. The seasonal surplus data are used for the third constraint.

4.2.2 Net Energy Output

The optimizing variables are separation pressure and condensing pressure levels for the low pressure turbine, same as for the net power optimization. The same non-linear constraints are used for the net energy optimization as for the net power optimization of the LPT cycle.

4.2.3 Economic Analysis

The setup of the optimization of levelized cost of electricity was the same as for the net energy output optimization. The only difference was the added economic calculations and the output value of the objective function.

4.3 Assumptions

For the optimization of both bottoming cycles, certain assumptions are made regarding the thermodynamic simulations and components. The assumptions are listed below.

4.3.1 Thermodynamic Modelling

The following assumptions are made for the thermodynamic calculations and processes for both ORC and LPT cycle:

- The “dead-state” in the exergy calculations was taken as T = 10°C, P = 1 atm
- All heat transfer processes where assumed isobaric
- No heat was lost to the environment during heat transfer processes
- All processes consuming or producing work and generating electricity were assumed non-isentropic and the losses defined with isentropic and mechanical efficiencies
- Mixing and separation were considered as isobaric and isenthalpic processes
- No frictional losses in pipelines were assumed

Six working fluids were chosen, see T-s diagram in Figure 4.1. Neither superheating nor trans-critical heating is assumed in the static thermodynamic models.

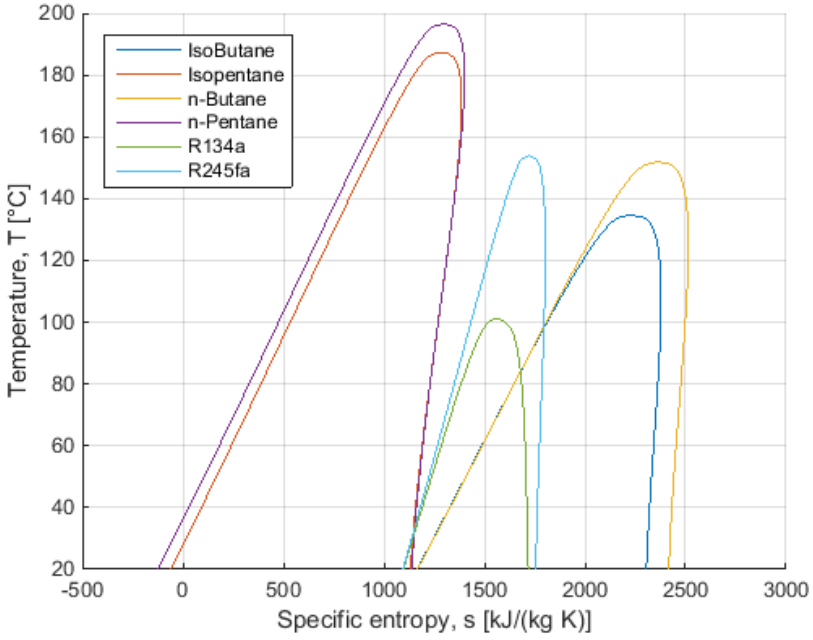

Figure 4.1: T-s diagram of saturations curves of working fluids chosen for this study. A recuperator was only prevalent in the ORC setups for the Pentane isomers, see slope of the vapor saturation curve

4.3.2 Components

Isentropic and mechanical efficiencies were assumed for the turbines, generators, pumps, fans and motors. The efficiencies were assumed from Dickson & Fanelli (2013) and DiPippo (2012).

Table 4.1: Isentropic and mechanical efficiencies for different components

Component	Efficiency, theory	Efficiency, chosen
Turbines	75-90%	85%
Pumps and Fans	40-60%	50%
Generators and Motors	90-98%	96%

Assumptions were made for pinch points in heater, boiler, recuperator and condenser. Pinch point is defined as the lowest temperature difference between two fluids while heat transfer takes place, when the hot fluid is cooled down while the cold fluid is heated up. In the heat transfer process, no pinch violations are allowed in the system. The pinch points were assumed from Bejan et. al (1996), Dickson & Fanelli (2013) and DiPippo (2012). A uniform pinch point for all heat exchangers was chosen as 7°C.

To calculate the heat transfer area for each heat exchanger, an overall heat transfer coefficient, U, was assumed for different heat exchangers. The coefficients were assumed from Sinnott (2005). The types of shell and tube heat exchanger were chosen from the fact that some of them had to be cleaned on a regular basis. The cleaning consists of removal of precipitated amorphous silica scales due to the cooling of brine. The floating head and kettle vaporizer are easy to clean due to the reason that tubes-side is removable and tubes can be replaced. The U-Tube type can be cleaned but not as easily as the former two. It is possible to clean the fixed head type but it is not suggested (Sinnott, 2005).

Table 4.2: Types of heat exchangers and their assumed overall heat transfer coefficients

Component	Type	U [W/(m^2 K)], theory	U [W/(m^2 K)], chosen
Heater	Floating head	150-1500	1200
Boiler	Kettle vaporizer	900-3000	2000
Recuperator	Fixed head	150-1500	1200
Cond., ORC	U-Tube	300-1500	1200
Cond., LPT	U-Tube	1500-4000	2000

Certain assumptions were made for the cooling cycle, the components within it and the evaporative cooling process. The assumptions for the steady–state processes are listed below:

- The cooling water enters the condenser at 20-21°C and warms up to 40°C
- Air coming into the cooling tower is at 5°C
- Air going out of the cooling tower is at 30°C, 10°C below the incoming cooling water

- The relative humidity of air coming into the cooling tower is assumed 65%
- The relative humidity of air going out of the cooling tower is assumed 95%
- The work done by the fan, Equation (3.22), was calculated from the dynamic pressure change of air, $0{,}5\rho v^2$. Two cooling water cells were assumed with 6m diameter fans
- Make-up water was added to assume steady-state operations
- Pressure increase in cooling water turbine is from 1 atm to 3 atm

Different components needed different types of material. Selection of material was needed for the material factors in the economical calculations. The components in contact with the brine were chosen as standard duplex stainless steel, S32205. Other were either chosen as austenitic stainless steel, R316 preferably, or carbon steel. The choice of material and other assumptions for different components in both bottoming cycles are listed below.

Table 4.3: Assumptions for different components in power generating bottoming cycles

Component	Type	Material	Reason
Separator - LPT	Horizontal	Duplex - 2205	Horizontal cheaper, in direct contact with brine
Recuperator - ORC	Fixed head	Carbon Steel	Does not need cleaning, carbon steel cheap
Heater - ORC	Floating head	Duplex - 2205	Needs cleaning, in direct contact with brine
Boiler - ORC	Kettle vaporizer	Duplex - 2205	Needs cleaning, in direct contact with brine
Condenser	U-Tube	S.S. – R316	Could be cleaned, oxygen rich water
Pumps	Centrifugal	S.S. – R316 Carbon steel	R316 for ORC, carbon steel for cooling cycle
Motors	Electric motor	Carbon Steel	For pumps and fans, carbon steel cheap
Fans	Blower	Cast aluminum	Small pressure increase, aluminum light and cheap

4.3.3 Economic Analysis

As before mentioned, the economic analysis of a bottoming cycle is a preliminary feasibility study and should be interpreted with a certain degree of uncertainty. The effect of inflation

was not considered in the LC calculations and the total CAPEX was assumed twice the cost of the equipment. Other assumptions are listed below.

Table 4.4: Assumptions for levelized cost of electricity (Bejan et al., 1996) (DiPippo, 2012)

	$CAPEX_{tot}$	**i in CRF**	**n in CRF**
Equity	30%	12 – 18%	25 yr.
Loan	70%	6%	25 yr.

5 Results

All results for from surplus availability calculations and thermodynamic optimizations are presented in the following section. The seasonal surplus is maximized at Nesjavellir while district heat production is maximized at Hellisheiði. The seasonal surplus is calculated for four different scenarios, one present and three future scenarios using certain assumptions. The maximized seasonal surplus for the present scenario is then used as input data for all thermodynamic models. Three optimization models are made for both bottoming cycles. Two different setups are optimized for the ORC, serial and parallel setups. Before interpreting the results, it is crucial to know the assumptions and the limitations of the models discussed in previous chapters.

5.1 Seasonal Surplus

A stepwise model was setup so heat would be produced at Hellisheiði instead of Nesjavellir. Consequently, seasonal surplus would be maximized at Nesjavellir while district heat production would be maximized at Hellisheiði. Both geothermal plants produce at minimum capacity when demand for district heating is low, e.g. during summer time. When minimum capacity from Nesjavellir and Hellisheiði is not enough, more district heat is produced at Hellisheiði, up to a safe production limit. The safe production limit was taken as approximately 90% of the maximum limit, so the system at Hellisheiði would not be under too much strain for a long period. When demand is greater than the minimum capacity at Nesjavellir and the safe capacity at Hellisheiði, more heat is produced at Nesjavellir, up to the maximum production capacity.

Table 5.1: Production capacity at Nesjavellir and Hellisheiði CHP plants (Júlíusson et al., 2016)

Location	**Min [kg/s]**	**Safe [kg/s]**	**Max [kg/s]**
Nesjavellir, Present	600	-	1350
Hellisheiði, Present	200	600	650
Hellisheiði w. Expansion	200	900	1000

A present scenario and three different future scenarios of heat demand are calculated. According to researchers at ON Power, the yearly increase in heat demand is 1.5%, interpreted as even throughout the year (Júlíusson et al., 2016). The surplus heat at Nesjavellir is maximized for all heat demand scenarios. The present scenario used original data as demand. The future scenarios are calculated demand in 2020 and 2030 without an expansion at Hellisheiði and the last scenario with demand in 2030 with the expansion in heat production at Hellisheiði.

Similar results are found when comparing the district heat production from present demand, Figure 5.1, to the production in 2030 with the expansion at Hellisheiði. The changes in low district heating demand are negligible while the heat production increases more in the latter scenario during colder months, from December to March.

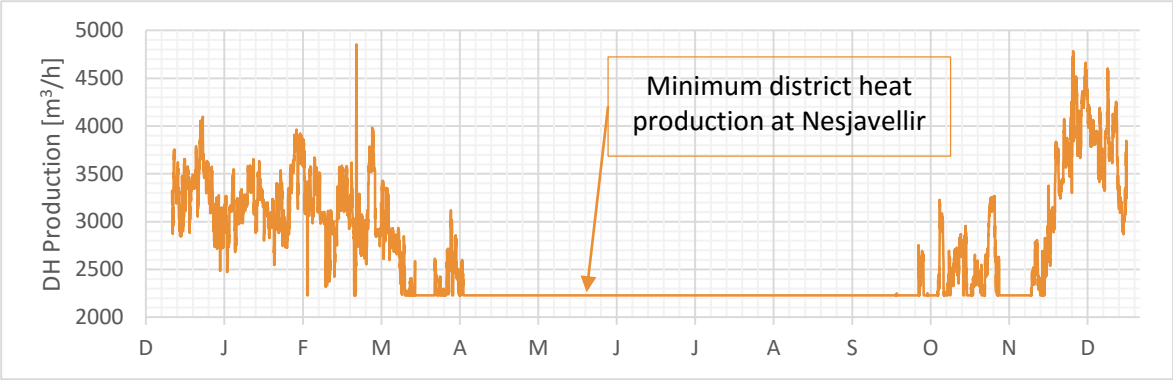

Figure 5.1: Calculated district heat production at Nesjavellir with present demand

Figure 5.2: Seasonal surplus at Nesjavellir with present demand. The surplus heat is calculated from the mass flow rate of the brine, the upper temperature limit of the brine and the lower temperature limit, 80°C

The seasonal surplus is the separated brine and is shown in thermal energy units. The surplus is calculated from the mass flow rate of the brine, the upper temperature limit of the brine and the lower temperature limit, 80°C. The changes in availability of seasonal surplus are seen in Table 5.2. Availability refers to the ratio when certain amount of energy is available throughout one year. There is more notable difference in availability of seasonal surplus when comparing present scenario with future scenarios, 2020 and 2030, without an expansion in heat production at Hellisheiði. Figures of district heat production and amount of seasonal surplus for future scenarios are found in Appendix II.

Table 5.2: Availability of seasonal surplus at Nesjavellir, all demand scenarios

Availability of Surplus	**Present**	**2020**	**2030**	**2030 w. exp.**
60 MW_{th} or more	64.2%	56.4%	45.6%	62.9%
40 MW_{th} or more	90.3%	75.8%	59.2%	81.7%

Results shown in Table 5.2 indicate that less and less seasonal surplus will be available at Nesjavellir. With an expansion at Hellisheiði, current availability of seasonal surplus could be prolonged up until 2030. The expansion assumed in this study was 66%, from 133 MW_{th} to 220 MW_{th}. The future expansion of heat production at Hellisheiði is still in its first stages. The expansion could be up to 400 MW_{th} but has not been confirmed (Júlíusson et al., 2016). Nonetheless, an expansion of some size would be beneficial for power generation from seasonal surplus at Nesjavellir CHP plant.

The thermal energy within the separated brine is used as input data for the ORC while it is used as a constraint for the LPT cycle. The brine is cooled down in the ORC but flashed in the LPT cycle and only the vapor portion utilized. Therefore, the representation of the seasonal surplus is more convenient for the ORC than the LPT cycle.

For the serial ORC setup, all of the brine is led through the boiler and heater when in operation. The brine begins at 195.1°C and is cooled down to a level which is calculated from the available seasonal surplus, see the lower temperature in Figure 5.3. For the parallel ORC setup, the mass flow rate of brine is split up. The total mass flow rate of brine at Nesjavellir is approximately 230 kg/s (Kjartansson, 2015). During periods of low heat demand, more than half of the mass flow of brine is utilized in the ORC. The availability of mass flow rate for the parallel ORC setup is represented in Figure 5.4.

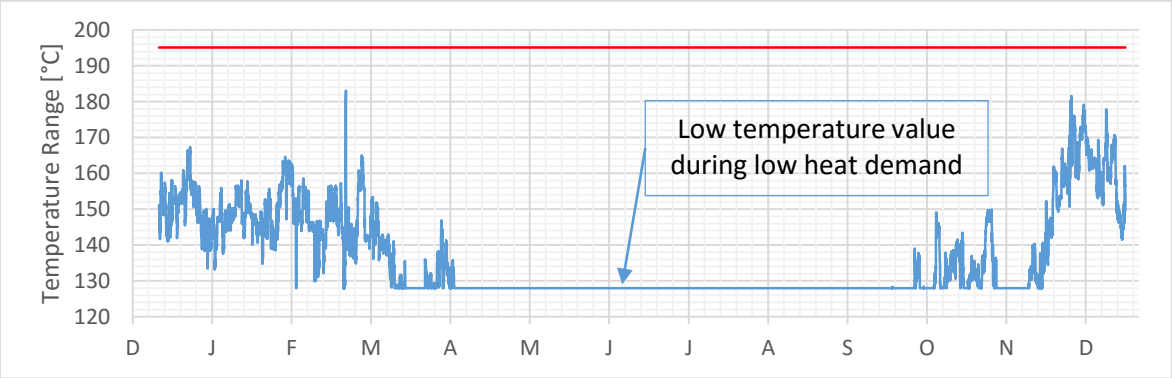

Figure 5.3: Serial ORC setup. The red line represents the higher temperature value of the brine, 195.1°C. The blue line represents the lower temperature value for the brine while fulfilling the demand for district heat. In summer time, the total mass flow of brine is allowed to be cooled down to approximately 130°C

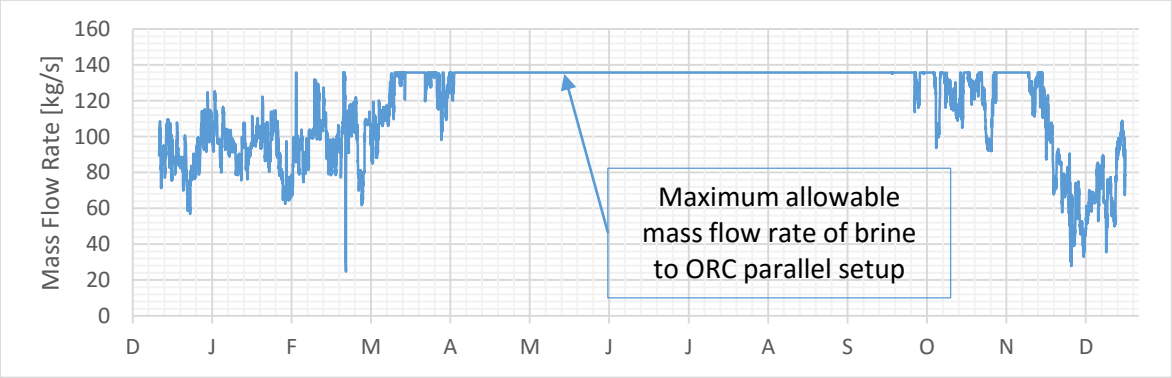

Figure 5.4: Parallel ORC setup. Available mass flow rate of separated brine. During summer time, most of the brine is led through the ORC, cooling the almost 140 kg/s of brine from 195.1°C down to 90°C

5.2 Organic Rankine Cycle

The calculated seasonal surplus data was used as input for the ORC simulations and optimizations. For all of the optimization setups, the values x_1 and x_2 were used as optimizing parameters, see Equations (4.1) and (4.2). Six ORC working fluids are optimized during simulations, Isobutane, Isopentane, n-Butane, n-Pentane, R134a and R245fa. The results are depicted in figures and listed in tables. The numbers in the following diagrams refer to a locations according shown in Figure 3.1.

5.2.1 Net Power Output

The net power output is the maximum net electrical power produced by the ORC. Contour were made to verify the results of the optimization function, fmincon. The contours showed either all solutions or all legal solutions with the optimizing parameters, x_1 and x_2, in the range of [0;1]. A legal solution is when all non-linear constrains are fulfilled. An illegal solution was taken as zero net power output, see Figure 5.5. When comparing the optimized solutions gotten from the models to the contours showing legal solutions, it is clear that the models find local minima for all working fluids considered in this study. The model simulated and optimized for both ORC setups, the serial and the parallel. The results for the serial setup are shown first, then the results for the parallel setup.

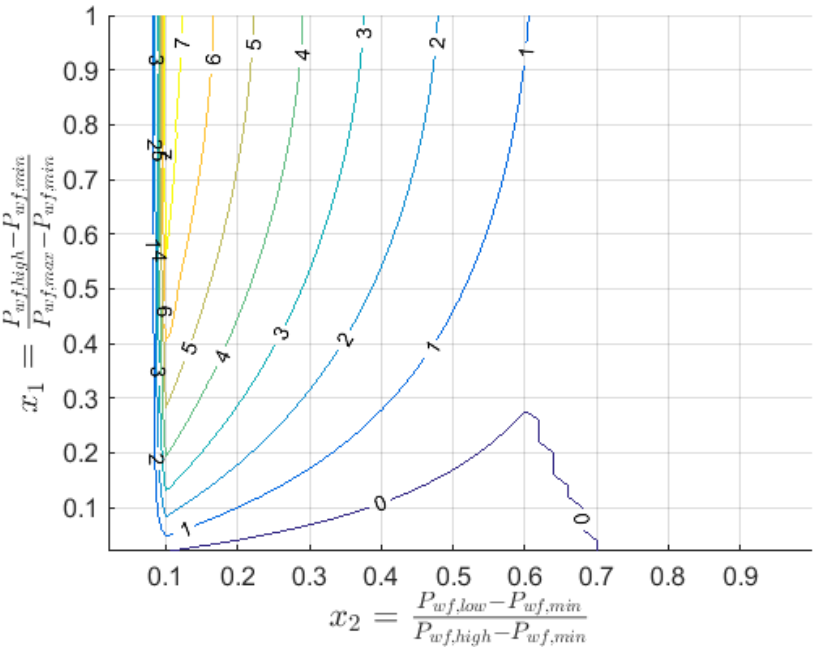

Figure 5.5: All legal solutions within the range of optimizing parameters for the ORC serial setup with R245fa as working fluid. Lines represent net power output in MW_e. Legal is referring to fulfillment of non-linear constraints. If not all constraints are fulfilled, the net power output was taken as zero

The optimized net power output for all working fluids in the serial setup are found in Table 5.3. After optaining optimum results, it is clear that n-Pentane and Isopentane are the two working fluids which give the best results for the serial setup. They have the most net power output, they have the greatest efficiencies and they have the lowest high pressure values which could decrease the cost of pipelines. It should be noted that they are also the only working fluids with a recuperator in the ORC serial setup.

Table 5.3: Optimized net power output for ORC serial setup

Working Fluids	$\dot{W}_{net}$ **[MW$_e$]**	**P$_{wf,high}$ [bar$_a$]**	**P$_{wf,low}$ [bar$_a$]**	**First Law Efficiency η_I**	**Second Law Efficiency η_{II}**	**Recup.**
Isobutane	6.3	32.1	6.2	9.4%	14.9%	No
Isopentane	10.6	22.5	1.8	15.8%	25.1%	Yes
n-Butane	7.6	33.5	4.4	11.4%	18.0%	No
n-Pentane	**10.7**	**17.9**	**1.4**	**16.0%**	**25.2%**	**Yes**
R134a	3.6	36.3	12.2	5.4%	8.6%	No
R245fa	7.8	31.8	3.0	11.7%	18.5%	No

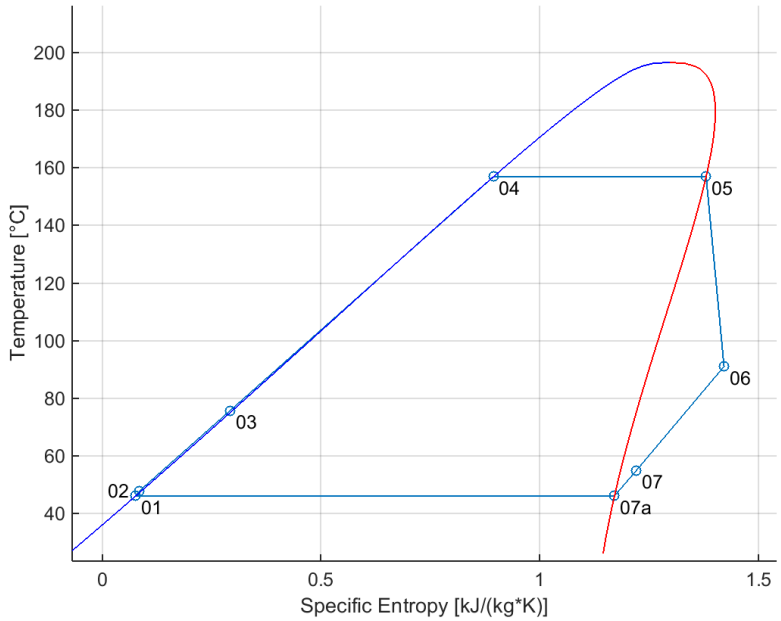

Figure 5.6: T-s diagram of the ORC serial setup with n-Pentane as working fluid. Dark blue line and red line represent the saturation curve of n-Pentane. Light blue lines represent the ORC process. Condensation takes place from 07 to 01, with 07a noting when the working fluid becomes saturated vapor

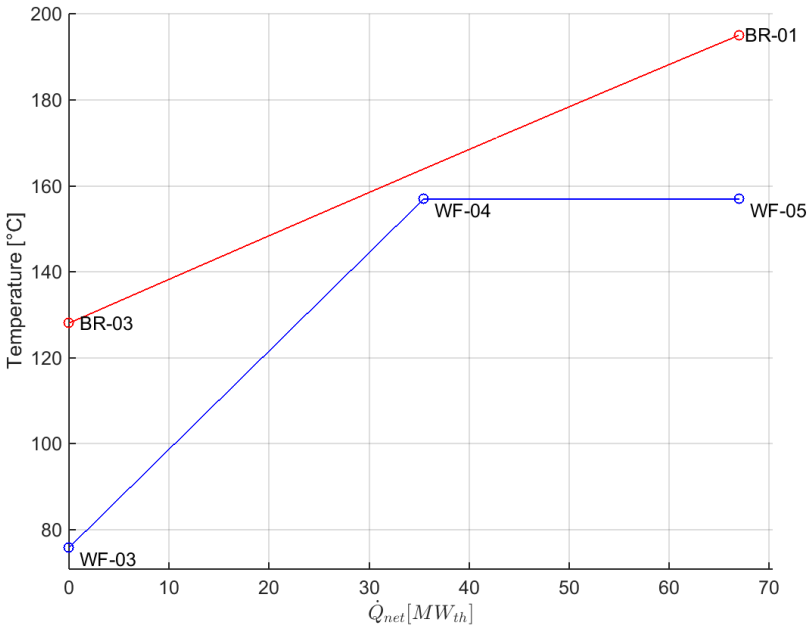

Figure 5.7: T-Q diagram of heat transfer process in the heater and boiler in the ORC serial setup with n-Pentane as working fluid

The optimized solutions for net power output of ORC parallel setup are found in Table 5.4. The net power output does not change for the butane isomers nor the refrigerants but is does decrease by roughly 20% for the Pentane isomers. This causes a drop in first law efficiency for both n-Pentane and Isopentane. On the other hand, all working fluids increase in second law efficiency, by 25% for Pentane isomer fluids and 40-60% increase for others.

Table 5.4: Optimized net power output for ORC parallel setup

Working Fluids	$\dot{W}_{net}$ **[MW$_e$]**	**P$_{wf,high}$ [bar$_a$]**	**P$_{wf,low}$ [bar$_a$]**	**First Law Efficiency η_I**	**Second Law Efficiency η_{II}**	**Recup.**
Isobutane	6.3	32.1	6.2	9.4%	23.1%	No
Isopentane	**8.45**	**12.2**	**1.8**	**12.6%**	**31.0%**	**Yes**
n-Butane	7.6	33.5	4.4	11.4%	28.0%	No
n-Pentane	8.3	9.4	1.4	12.3%	30.3%	Yes
R134a	3.6	36.3	12.2	5.4%	13.3%	No
R245fa	7.8	31.8	3.0	11.7%	28.7%	No

The change in second law efficiencies is explained by looking again at Equation (3.6) and understanding what exergy losses represents. For the heat transfer processes, the exergy losses are defined as the difference between ingoing and outgoing exergy. The exergy losses were calculated slightly higher for the heater and boiler in the ORC serial setup than the parallel setup. This could also be interpreted by looking at a T-Q diagram and having the integral definition of exergy in mind. The exergy loss in the heat transfer processes can be defined as the area between the hot fluid and the cold fluid (Dickson & Fanelli, 2013).

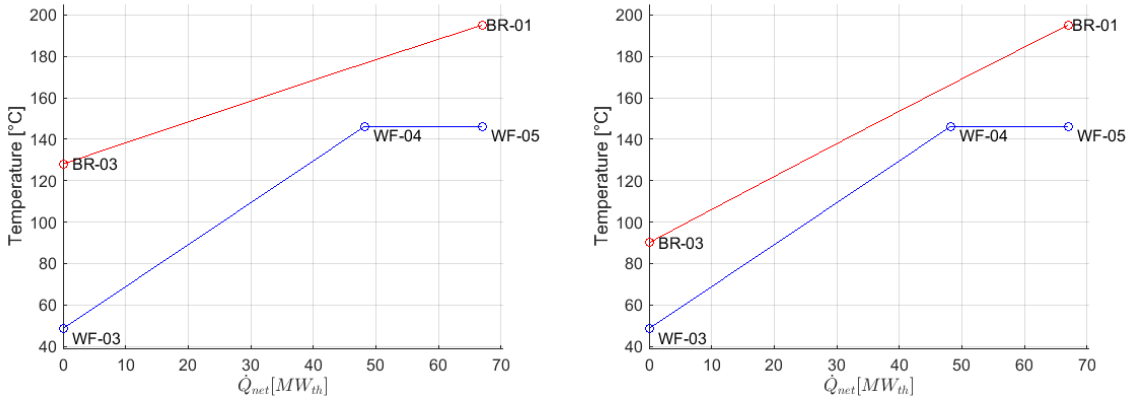

Figure 5.8: Comparison between T-Q diagrams of the serial setup (left) and the parallel setup (right) for ORC with R245fa as working fluid. Second law efficiency increases by 55% from the serial setup to the parallel setup. Notice the difference in area between the lines of separated brine (red) and R245fa (blue)

Apart from being the only fluids with decreased net power output, n-Pentane and Isopentane are still the best performing working fluids. They both have much lower high pressure value than other fluids which give a cheaper piping system and a cheaper pump, more on economical calculations in 5.2.3. Nonetheless, it should be noted that R245fa is without a recuperator and only has slightly worse results than the Pentane isomers and therefore should be considered. The parallel ORC with Isopentane have slightly better results than n-Pentane.

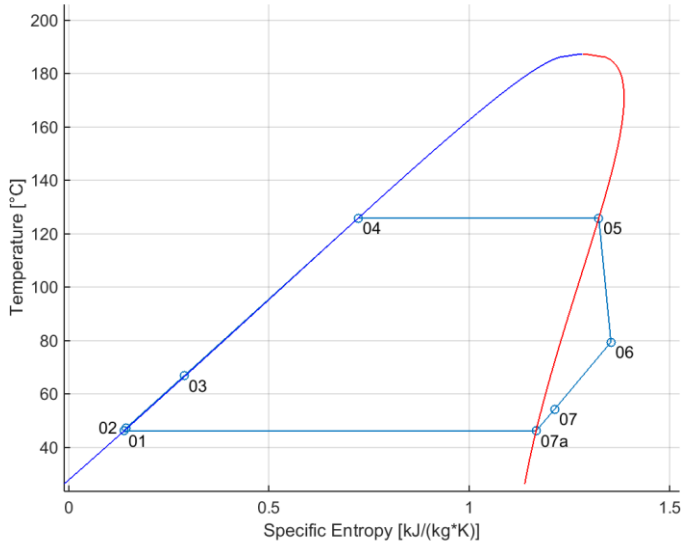

Figure 5.9: T-s diagram of the ORC parallel setup with Isopentane as working fluid. Dark blue line and red line represent the saturation curve of Isopentane. Light blue lines represent the ORC process

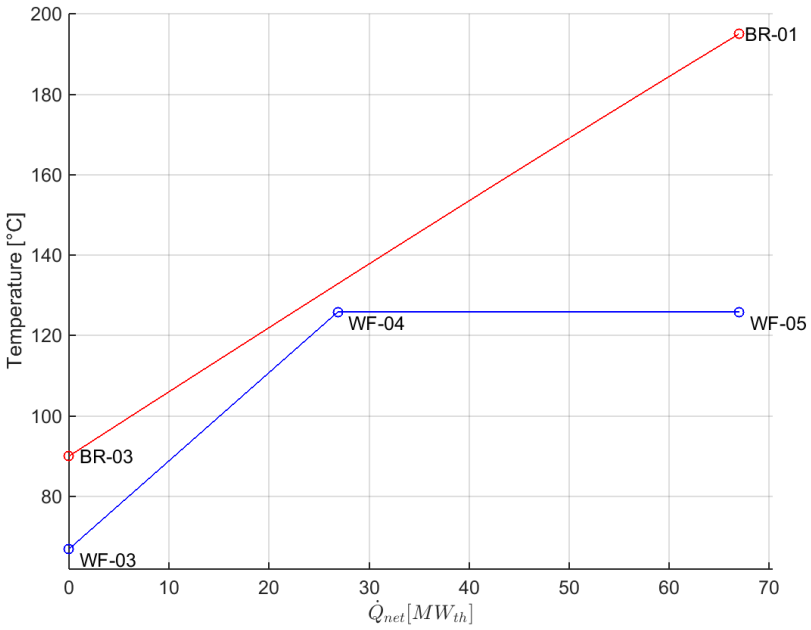

Figure 5.10: T-Q diagram of heat transfer process in the heater and boiler in the ORC parallel setup with Isopentane as working fluid

5.2.2 Net Energy Output

There are more than one local maxima for the simulations and optimization of net energy output. The availability of seasonal surplus is taken into consideration. The availability represents the proportion of the year which the ORC is in full operation. During periods of low heat demand, the seasonal surplus stored in the brine is utilized by the ORC. When heat demand increases above a certain limit, the mass flow of brine is redirected from the ORC and utilized only for district heat production. No off-design operation of the ORC was considered. All four setups were optimized.

Table 5.5: Optimized net energy output for ORC serial setup with a single turbine

Working Fluids	W_{net} **[GWh$_e$]**	$\dot{W}_{net}$ **[MW$_e$]**	**Available [%]**	**P$_{wf,high}$ [bar$_a$]**	**P$_{wf,low}$ [bar$_a$]**	**First Law Efficiency η_I**	**Second Law Effic. η_{II}**
Isobutane	32.4	5.9	62.4	32.2	6.2	9.5%	14.0%
Isopentane	56.6	7.6	83.4	26.5	1.8	16.6%	18.0%
n-Butane	39.0	7.2	61.5	33.5	4.4	11.6%	17.2%
n-Pentane	**56.3**	**8.7**	**73.5**	**21.2**	**1.4**	**16.9%**	**20.6%**
R134a	19.2	2.8	78.9	36.3	12.2	5.7%	6.6%
R245fa	40.0	7.3	62.9	31.8	3.0	11.8%	17.4%

The availability ranges from 57.9% to 100%, with maximum surplus heat being utilized for the ORC when availability is at a minimum. The working fluids showing the most net energy output were the Pentane isomers, n-Pentane and Isopentane. The net power output and second law efficiencies decrease compared to optimizations of ORC serial setup. On the other hand, the two working fluids increase in both high pressure value and all increase in first law efficiency. These changes can be understood by looking at a T-Q diagram of the heater and boiler, see Figure 5.11, and by calculating the exergy losses. With more availability, less thermal power is utilized for the ORC bottoming unit. For the Pentane isomers in the ORC serial setup, less heat being extracted from the brine means possibility for an increase in high pressure level. On the other hand, utilization of less heat than in 5.2.1 leads to an increase in exergy losses and a decrease in both net power output and second law efficiency.

The Pentane isomers give the best performance for net energy optimization of the ORC serial setup, with n-Pentane having slightly better results. The potential electric energy production for the Pentane isomers is up to 56 GWh_e for one year. The energy would be produced 70-80% of the year, with net power output of 7.5-9 MW_e and total installed capacity of 8.5-10 MW_e. The decrease in net power output between optimizations is a result of decreased mass flow rate of working fluids. Results for n-Pentane are shown below. The T-s diagram is similar to the one in Figure 5.6 and therefore not depicted.

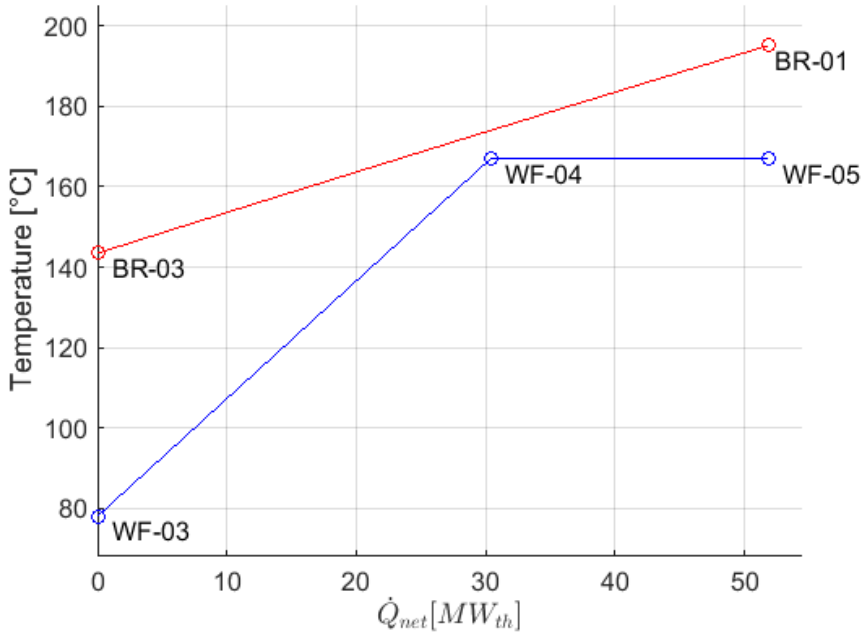

Figure 5.11: T-Q diagram of heat transfer process in the heater and boiler in the ORC serial setup with n-Pentane as working fluid. By comparing with Figure 5.7, the area between lines has increased. The exergy losses are more in the net energy optimization than the net power optimizations, leading to a lower η_{II}

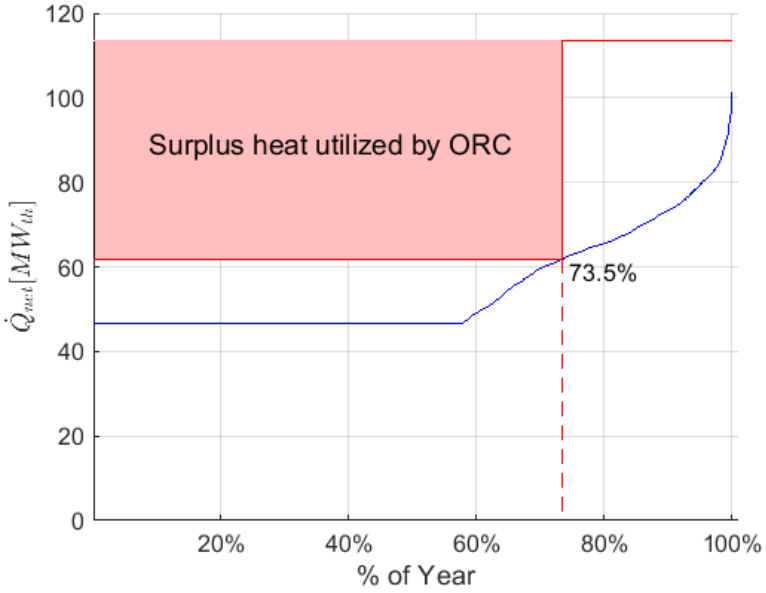

Figure 5.12: Availability of ORC. The blue line represents load duration curve for the district heat production needed for Reykjavík. The red line represents the thermal energy available for district heat production. Dashed line shows the availability of the ORC serial setup with n-Pentane as working fluid. When the demand for district heat surpasses the heat available, the ORC unit is shut down and all brine utilized for district heating

The results from the net energy optimizations for ORC parallel setup can be seen in Table 5.6. As in 5.2.1, the net power output and first law efficiency decrease for the parallel setup while the second law efficiencies increase. That is explained by less exergy losses for the parallel setup. The working fluids with the best performance are again the Pentane isomers, with Isopentane having slightly better results. It should be noted that optimized solution for R245fa has no recuperator and only slightly worse results than Pentane isomers. The load duration curve of district heat production and availability of the ORC parallel setup for the Isopentane are similar to Figure 5.12. The T-s diagram for Isopentane is similar to Figure 5.9 and therefore not depicted.

Table 5.6: Optimized net energy output for ORC parallel setup with a single turbine

Working Fluids	W_{net} **[GWh$_e$]**	$\dot{W}_{net}$ **[MW$_e$]**	**Available [%]**	**P$_{wf,high}$ [bar$_a$]**	**P$_{wf,low}$ [bar$_a$]**	**First Law Efficiency η_I**	**Second Law Effic. η_{II}**
Isobutane	32.7	4.6	80.9	32.2	6.2	9.7%	23.8%
Isopentane	**43.4**	**6.1**	**81.2**	**12.2**	**1.8**	**12.9%**	**31.6%**
n-Butane	39.3	7.6	81.3	33.5	4.4	11.7%	28.6%
n-Pentane	42.4	6.0	80.8	9.4	1.4	12.6%	30.9%
R134a	19.1	2.8	77.6	36.3	12.2	5.7%	14.0%
R245fa	40.3	5.7	81.0	31.8	3.0	11.9%	29.3%

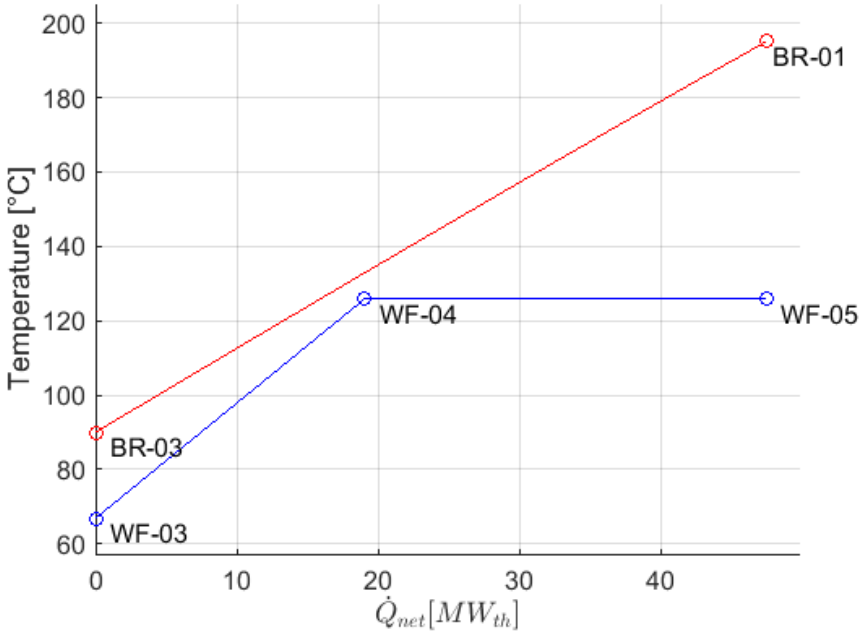

Figure 5.13: T-Q diagram of heat transfer process in the heater and boiler in the ORC parallel setup with Isopentane. The exergy losses are less in the ORC parallel setup than for the ORC serial setup, leading to an increase in second law efficiency

Another net energy optimization was simulated for both serial and parallel setups, having two turbines simulated instead of a single turbine. When heat demand increases, only one of the turbines, T2, would have to shut down, allowing the other, T1, to produce for a longer period. When heat demand increases further, turbine T1 shuts down as well and brine is directed away from the ORC. Therefore, increased amount of net energy output could be achieved. The drawback is increased cost. The results from the net energy optimization for ORC serial setup are listed in Table 5.7. $\dot{W}_{T1}$ and $\dot{W}_{T2}$ stand for total installed capacity for each turbine with T1 generating for a longer period.

Table 5.7: Optimized net energy output for ORC serial setup with two turbines, T1 and T2

Working Fluids	W_{net} **[GWh$_e$]**	$\dot{W}_{net}$ **[MW$_e$]**	$\dot{W}_{T1}$ **[MW$_e$]**	**Avail.-T1 [%]**	$\dot{W}_{T2}$ **[MW$_e$]**	**Avail.-T2 [%]**
Isobutane	42.6	6.3	5.3	89.6	3.5	57.9
Isopentane	72.0	10.6	7.2	91.4	5.1	57.9
n-Butane	51.7	7.7	6.4	86.5	3.4	57.9
n-Pentane	**72.5**	**10.7**	**6.8**	**92.7**	**5.3**	**57.9**
R134a	24.3	3.6	4.1	86.5	2.3	57.9
R245fa	53.1	7.8	5.8	91.5	4.1	57.9

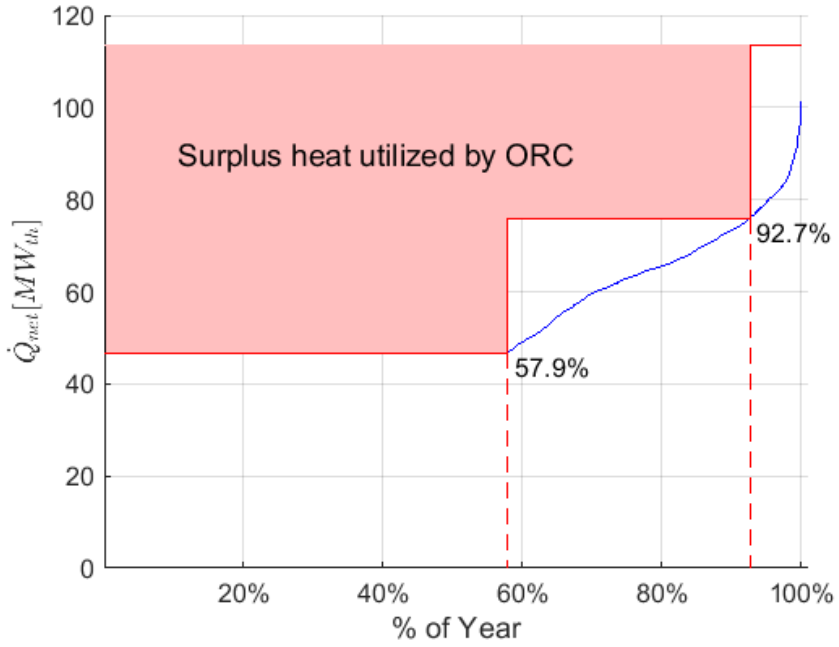

Figure 5.14: Availability of two turbines in ORC serial setup. The blue line represents load duration curve for the district heat production needed for Reykjavík. The red line represents the thermal energy available for district heat production. Dashed line shows the availability of the turbines in ORC serial setup with n-Pentane

The Pentane isomers show the best results. The benefit of having two turbines in the serial ORC setup is that almost 30% more electric energy could be produced. For all working fluids, the first turbine operated for roughly 90% of the year. The second turbine was always shut down then when heat demand increased above minimum heat production at Nesjavellir.

As for the parallel connection, the working fluids with best performance are the Pentane isomers. The R245fa refrigerant had also good results and should be considered. The benefit of having two turbines in the parallel ORC setup is that more than 30% more electric energy could be produced. The second turbine was always shut down then when heat demand increased above minimum production at Nesjavellir, see Table 5.8 below.

Table 5.8: Optimized net energy output for ORC parallel setup with two turbines, T1 and T2

Working Fluids	W_{net} **[GWh$_e$]**	$\dot{W}_{net}$ **[MW$_e$]**	$\dot{W}_{T1}$ **[MW$_e$]**	**Avail.-T1 [%]**	$\dot{W}_{T2}$ **[MW$_e$]**	**Avail.-T2 [%]**
Isobutane	42.8	6.3	5.1	92.1	3.7	57.9
Isopentane	**57.4**	**8.5**	**5.6**	**92.1**	**4.1**	**57.9**
n-Butane	50.6	7.6	6.8	84.1	3.2	57.9
n-Pentane	56.1	8.3	5.4	91.9	3.9	57.9
R134a	24.2	3.6	4.2	86.2	2.2	57.9
R245fa	53.1	7.8	5.8	91.4	4.1	57.9

5.2.3 Levelized Cost of Electricity

There are more than one local minima for the simulations and optimization of levelized cost of electricity, LC. The availability of seasonal surplus is taken into consideration. Four scenarios are simulated, as in the net energy optimization. The four LC optimization included two ORC setups, serial and parallel, and both one and two turbines. The optimization process for the LC was slower than for the net energy output due to an economic calculation function being called within the objective function. The equations listed in 3.5 and Appendix I were used for the economic estimations. The equity ratio was assumed 30%-70% with rate of return as 18%, interest rate as 6% and lifetime of the ORC bottoming unit as 25 years. The choice of material and other assumptions are listed in Table 4.3.

Table 5.9: Optimized levelized cost of electricity for ORC serial setup with one turbine

Working Fluids	**LC [ISK/kWh$_e$]**	**W_{net} [GWh$_e$]**	**$\dot{W}_{net}$ [MW$_e$]**	**Available [%]**	**Cost of $\dot{W}_{net}$ [MUSD/MW$_e$]**
Isobutane	4.59	27.2	3.3	95.1	2.62
Isopentane	3.34	42.9	5.1	96.5	**1.93**
n-Butane	3.96	30.1	3.5	97.4	2.32
n-Pentane	**3.26**	**43.9**	**5.2**	**96.7**	**1.89**
R134a	6.92	14.4	1.7	98.1	3.98
R245fa	3.98	37.7	4.7	91.5	2.11

Pentane isomers have the best results from the LC optimizations, for both serial and parallel ORC setups and one turbine. The simulations with the serial setup have slightly favorable results than with the parallel setup. Although LC was optimized, the total cost per net power output should also be considered, last columns in Table 5.9 and Table 5.10. The difference between the Pentane isomers is almost negligible. For the serial setup, both produce most net energy and have the lowest LC, ranging from 3.2 to 3.4 ISK/kWh$_e$. The levelized cost of electricity was calculated for the Pentane isomers after the net energy optimization with one turbine. The LC for the Pentane isomers in the serial setup ranged from 5.0-5.3 IKS/kWh$_e$ while producing up to 30% more electrical energy than for the LC optimization.

As for the parallel setup, the performances between four working fluids is within the margin of error. The four fluids giving the best results for the parallel setup are the Pentane isomers, n-Butane and R245fa. The levelized cost of electricity from those four working fluids ranges from 3.9 to 4.2 ISK/kWh$_e$. For the net energy optimization, the LC for these four working fluids in the parallel setup ranged from 5.6-6.5 IKS/kWh$_e$ while producing up to 25% more electrical energy than for the LC optimization with a single turbine.

Table 5.10: Optimized levelized cost of electricity for ORC parallel setup with one turbine

Working Fluids	LC [ISK/kWh$_e$]	W_{net} [GWh$_e$]	$\dot{W}_{net}$ [MW$_e$]	Available [%]	Cost of $\dot{W}_{net}$ [MUSD/MW$_e$]
Isobutane	4.70	25.3	3.0	97.2	2.74
Isopentane	**3.96**	**35.7**	**4.2**	**96.2**	**2.28**
n-Butane	4.19	32.5	3.9	96.1	**2.42**
n-Pentane	4.07	37.9	4.7	92.4	**2.26**
R134a	7.10	15.8	1.9	96.5	4.14
R245fa	4.14	36.1	4.4	92.4	**2.29**

The results for serial ORC setup with two turbines are similar to the LC optimization of the serial setup with a single turbine. When looking at results in Table 5.11 and comparing to results in Table 5.9, it is clear that the benefit of having two turbines in the serial setup diminishes in the LC optimization. Both turbines in the serial ORC setup are simulated with high availability for all working fluids, meaning decreased total installed capacity. The Pentane isomers give the best performance, having 3.2-3.4 IKS/kWh$_e$ and 1.9-2.0 MUSD/MW$_e$, similar for results with one turbine. The optimized solution for n-Pentane minimizes the installed capacity of T1 as much as possible, minimizing the cost. The levelized cost of electricity was also calculated for the Pentane isomers after the net energy optimization with two turbines. The LC for the Pentane isomers in the serial setup and two turbines ranged from 4.2-4.9 IKS/kWh$_e$. Although slightly higher LC, the net energy optimization produces up to 70% more electrical energy than for the LC optimization with two turbines in the serial setup, up to 72.5 GWh$_e$ per year.

Table 5.11: Optimized levelized cost of electricity for ORC serial setup with two turbines, T1 and T2

Working Fluids	LC [ISK/kWh$_e$]	W_{net} [GWh$_e$]	$\dot{W}_{net}$ [MW$_e$]	Avail. – T1 [%]	Avail. – T2 [%]	Cost of $\dot{W}_{net}$ [MUSD/MW$_e$]
Isobutane	4.57	27.5	3.3	95.1	95.1	2.61
Isopentane	3.39	45.7	5.4	96.7	95.0	**1.97**
n-Butane	4.03	34.6	5.5	80.8	80.7	2.21
n-Pentane	**3.24**	**45.3**	**5.4**	**100**	**96.7**	**1.88**
R134a	7.00	16.5	2.0	95.2	95.2	4.01
R245fa	3.88	34.6	4.2	94.4	94.4	2.20

The results for parallel ORC setup with two turbines are similar to the LC optimization of the parallel setup with a single turbine. When looking at results in Table 5.12 and comparing to results in Table 5.10, it is certain that the benefit of having two turbines in the parallel setup disappears in the LC optimization. Both turbines in the parallel setup are simulated with high availability for all working fluids. The ones with 100% availability have less than 0.1 MW_e of installed capacity, meaning the optimized solution minimizes one of the turbines. The Pentane isomers give the best performance with R245fa also being a contender. The LC was 3.8-4.2 IKS/kWh_e and the total cost per net power output was 2.2-2.4 $MUSD/MW_e$. Economic calculations were done for the net energy optimization of the two turbine parallel setup. The LC was 4,8-5,2 ISK/kWh_e and the cost per net power output was same as for two turbines, 2.2-2.4 $MUSD/MW_e$. Although slightly higher LC, the net energy optimization with two turbines parallel setup produces up to 60% more electrical energy than for the LC optimization with two turbines in the serial setup.

Table 5.12: Optimized levelized cost of electricity for ORC parallel setup with two turbines, T1 and T2

Working Fluids	**LC [ISK/kWh$_e$]**	**W_{net} [GWh$_e$]**	**$\dot{W}_{net}$ [MW$_e$]**	**Avail. – T1 [%]**	**Avail. – T2 [%]**	**Cost of $\dot{W}_{net}$ [MUSD/MW$_e$]**
Isobutane	4.81	29.8	3.5	96.2	93.0	2.76
Isopentane	3.96	35.7	4.2	96.2	96.2	2.28
n-Butane	4.39	38.7	4.9	91.8	88.0	2.41
n-Pentane	**3.84**	**56.9**	**6.9**	**100**	**94.7**	**2.19**
R134a	7.19	15.9	1.9	100	96.2	4.15
R245fa	4.13	36.6	4.4	95.0	92.8	2.35

These results, for two turbines in both setups, indicate that the LC optimization does not necessarily find the most efficient solution from the buyer's point of view. The small difference in LC between results for optimized net energy and optimized LC suggest that the former optimization is preferred. The rate of return was assumed 18% for the equity, with the equity ratio being 30%-70%. By lowering the rate of return down to 12-15%, the LC decreased for all four scenarios. The economic calculations were made to find out the economic feasibility of the ORC bottoming unit. The LC would have to be equal or lower than the current price of electricity before taxes for the ORC bottoming unit to be economically feasible. According to Júlíusson et al. (2016), the price of electricity before taxes is dependent on seasonal changes and demand, ranging from 3.5 to 5.5 ISK/kWh_e. The levelized cost of electricity, LC, with lower the rate of return; RoR, for net energy optimized solutions of all four setups are listed below.

Table 5.13:Levelized cost of electricity for net energy optimizations with different rates of return for equity

Optimization Scenario **Setup – Turbines – Working fluid**	**LC with RoR = 18% [ISK/kWh$_e$]**	**LC with RoR = 15% [ISK/kWh$_e$]**	**LC with RoR = 12% [ISK/kWh$_e$]**
Serial – One turbine – n-Pentane	5.00	4.65	4.31
Parallel – One turbine – Isopentane	5.59	5.19	4.81
Serial – Two turbines – n-Pentane	4.21	3.9	3.62
Parallel – Two turbines – Isopentane	4.89	4.55	4.21

According to the economic feasibility study, the optimized serial setup with two turbines is the most favorable option. The levelized cost of electricity does not take into account the cost of transportation nor the effect of inflation throughout each year. The distribution of total equipment purchased cost is shown in Figure 5.15. According to the assumptions and equations used in the economic calculations, the purchased equipment cost is distributed 54%-46% amongst the turbines plus generators and all other equipment, respectively. According to Guðmundsson (2016), the cost per net power output for an ORC unit is in the range of 2-2.5 MUS$/MW$_e$. The results from both the LC and net energy optimizations are lower than that range, indicating that the real cost for the ORC could be higher than the results indicate.

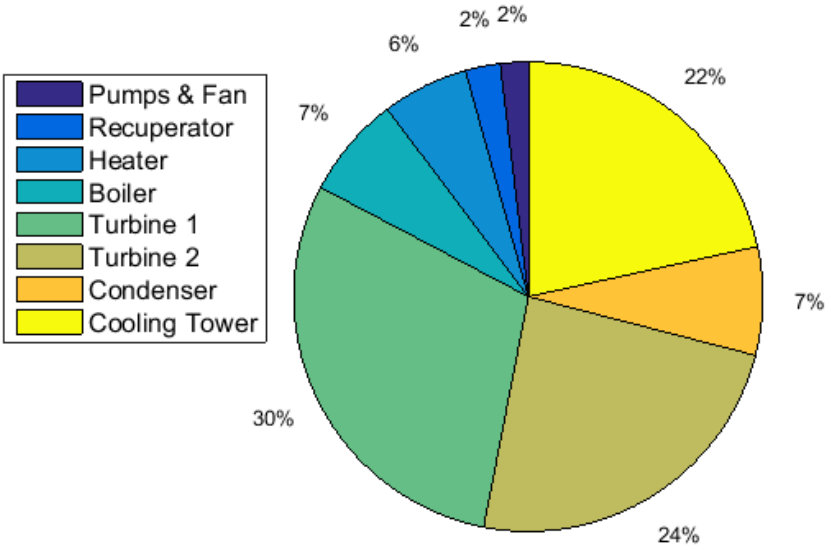

Figure 5.15: Distribution of purchased equipment cost for ORC serial setup with two turbines

5.3 Low Pressure Turbine Cycle

The calculated seasonal surplus data was used as input for the LPT cycle simulations and optimizations. For all of the optimization setups, the values x_1 and x_2 were used as optimizing parameters, see Equations (4.5) and (4.6). All optimization models had the same optimizing parameters but differed in non-linear constraints specified in 4.2. The numbers in the following diagrams refer to a locations shown in Figure 3.5.

5.3.1 Net Power Output

Surface contours were made to verify the results of the optimization function, fmincon. The contours showed all legal solutions with the optimizing parameters, x_1 and x_2. A legal solution is when all non-linear constrains are fulfilled. An illegal solution was taken as zero net power output, see Figure 5.16. When comparing the optimized solutions gotten from the models to the contours showing legal solutions, it is clear that the model finds a local minimum for the LPT net power output optimization. The results for the net power optimization are listed below in Table 5.14. The numbers in Figure 5.17 correspond to locations in Figure 3.5. Only about 12% of the mass flow rate of high pressure brine is separated into low pressure vapor, the rest stays as liquid. The results for net power output and second law efficiency are similar for the Pentane isomers in the serial ORC with a single turbine, see Table 5.3.

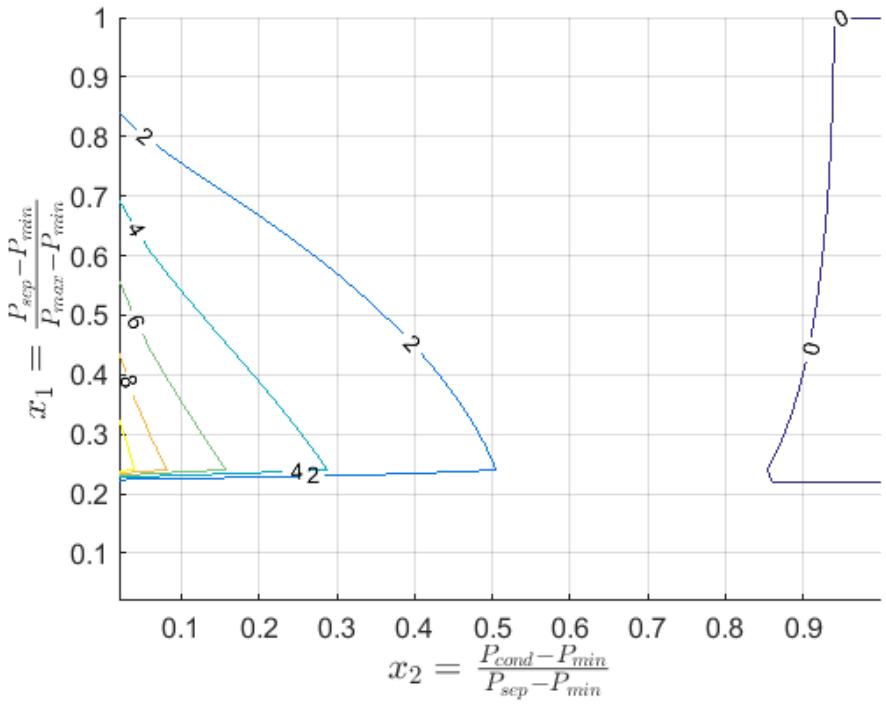

Figure 5.16: All legal solutions for LPT net power output within the range of optimizing parameters. Lines represent net power output in MW_e. Legal is referring to fulfillment of non-linear constraints. If constraints are not fulfilled, the output was zero

Table 5.14: Net power output optimization for LPT cycle

Optimization	$\dot{W}_{net}$ [MW_e]	$\dot{m}_{vap}$ [kg/s]	**P_{sep} [bar_a]**	**P_{cond} [bar_a]**	**Fist law eff. η_{II}** [%]	**Second law eff., η_{II}** [%]
LPT - NPO	10.4	28.1	3.10	0.11	15.2	24.5

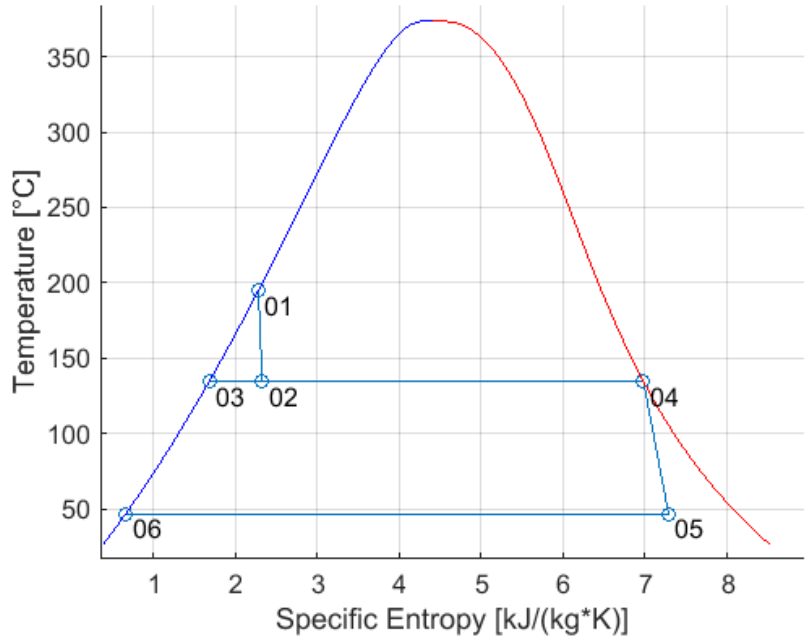

Figure 5.17: T-s diagram of the LPT cycle process optimized for net power output. The dark blue and red curves show the saturation curve of water. The numbers correspond to locations in Figure 3.5

5.3.2 Net Energy Output

Contours were made to verify the results of the optimization function, fmincon. The net energy optimization for the LPT behaved in the same manner as for the ORC. By lowering the total installed capacity, the availability of the LPT cycles increased. As for the ORC, no off-design operation of the LPT cycle were considered. As The results for the net energy optimization of the LPT are found below.

Table 5.15: Net energy output optimization for LPT cycle

Optimization	W_{net} [GWh_e]	$\dot{W}_{net}$ [MW_e]	**Avail. [%]**	**P_{sep} [bar_a]**	**P_{cond} [bar_a]**	**Second law eff., η_{II}** [%}
LPT - NEO	65.3	9.1	81.9	5.38	0.11	21.5

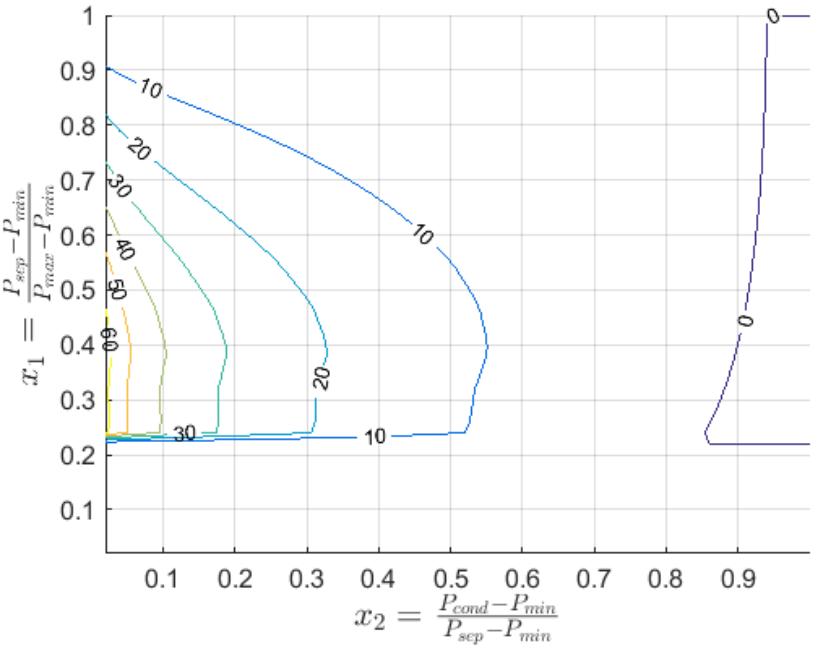

Figure 5.18: All legal solutions for LPT net energy output within the range of optimizing parameters. The lines represent net energy output in GWh_e

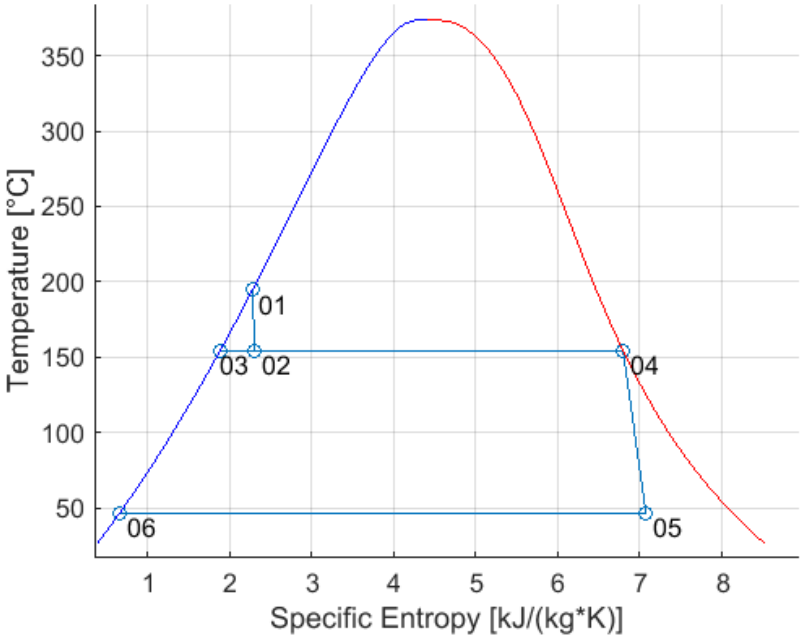

Figure 5.19: T-s diagram of the LPT process optimized for net energy output. The dark blue and red curves show the saturation curve of water. The numbers correspond to locations in Figure 3.5

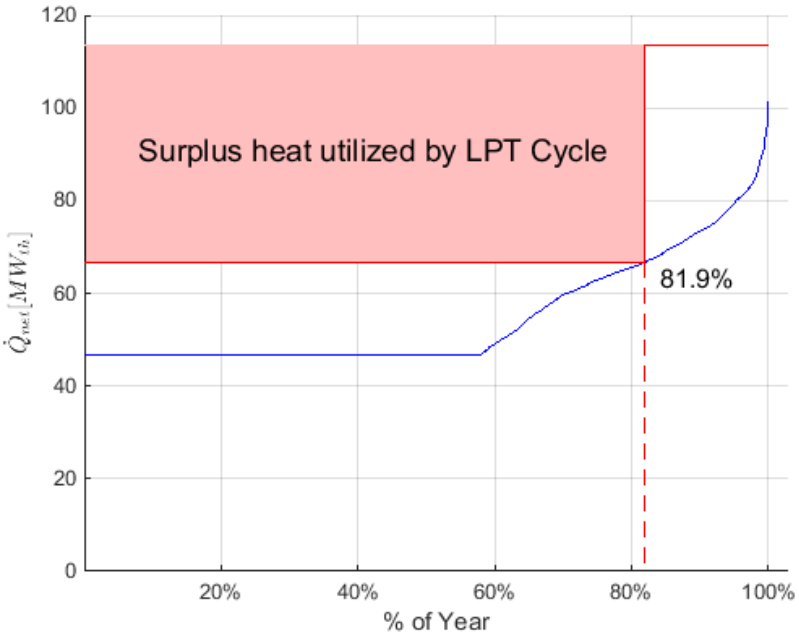

Figure 5.20: Availability of LPT cycle. The blue curve is load duration curve of district heat production from Nesjavellir. The red line represents the thermal energy available for district heat production and the dashed red line indicates the availability of the LPT cycle according to the net energy optimization

5.3.3 Levelized Cost of Electricity

There were more than one local minima for the simulations and optimization of levelized cost of electricity, LC. The availability of seasonal surplus was taken into consideration. The optimization process for the LC was more time-consuming than for the net energy output due to an economic calculation function being called within the objective function. The equations listed in 3.5 were used for economic calculations. The equity ratio was assumed 30%-70% with rate of return as 18%, interest rate as 6% and lifetime of the LPT bottoming unit as 25 years. The choice of material and other assumptions are listed in Table 4.3. The results for the LC optimization for the LPT were much more favorable than for the ORC. The results for the LC optimization of the LPT cycle are found below. The T-s diagram for the LC optimization is similar to Figure 5.19 and therefore not shown.

Table 5.16: Levelized cost of electricity and net energy optimizations for LPT cycle

Optimization	**LC [IKS/kWh$_e$]**	W_{net} [GWh$_e$]	$\dot{W}_{net}$ [MW$_e$]	**Avail. [%]**	**P$_{sep}$ [bar$_a$]**	**Cost of MW$_e$ [MUSD/MW$_e$]**
LPT - LC	3.38	64.4	8.6	85.5	5.77	1.74
LPT - NEO	3.52	65.3	9.1	81.9	5.38	1.73

In both optimizations, LC and net energy output, the levelized cost is within range of economic feasibility. The equity ratio was assumed 30%-70% with the rate of return as 18% and interest rate as 6%. The distribution of purchased equipment cost is similar to the ORC setup with two turbines. More than half of the cost relates to the turbine and generator, rest to separator, condenser and cooling cycle. According to Guðmundsson (2016), the cost per net power output for a well-head low pressure turbine cycle is in the range of 1.75-2.4 MUS$/$MW_e$. The results from both the LC and net energy optimization are at the lower end of that range, indicating that the real cost for LPT cycle could be higher than results show.

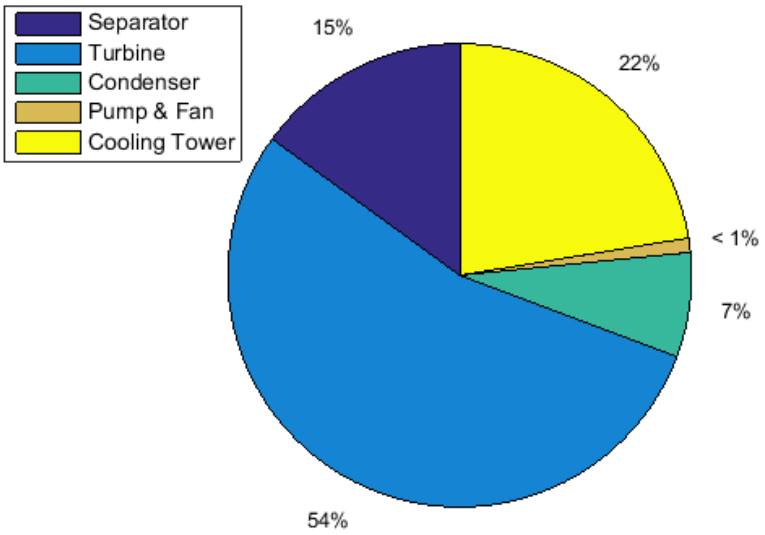

Figure 5.21: Distribution of purchased equipment cost for LPT cycle

6 Conclusions

According to the results of this study, there is an economic feasible way of exploiting the seasonal surplus available at Nesjavellir CHP plant. The optimized LPT bottoming cycle generates a little bit less electrical energy per year than the optimized ORC. For both ORC setups, the Pentane isomers had the best performances. The optimized solution for the serial ORC setup was with two turbines and using n-Pentane as working fluid. The total generated electricity throughout the span of one year was 72.5 GWh_e with the LC of 4.21 ISK/kWh_e while having the RoR as 18%. The optimized solutions for the parallel ORC setup was with two turbines and using Isopentane as working fluid. The total generated electricity was 57.4 GWh_e with the LC of 4.89 ISK/kWh_e. The optimized solutions for the LPT generated 64.4 GWh_e with the LC of 3.38 ISK/kWh_e.

The optimized LPT cycle was less expensive than the optimized ORC, with a slightly lower levelized cost of electricity. The LCs for the optimized solutions are in the range of the electricity prices before taxes, making both bottoming units economically feasible. On the other hand, the economic analysis is thought of as a preliminary feasibility study with some uncertainties. For both bottoming cycles, the cost per net energy output is at the lower end of the expected range obtained from Verkís Consulting Engineers (2016). That indicates that the cost estimates are generous and some unpredicted cost must be added to the economic analysis. This cost could originate from the cost of transportation, higher maintenance cost or some other unforeseeable cost often included in economic analyses.

Both corrosion and scaling are expected when utilizing the seasonal surplus at Nesjavellir. The corrosion rate is minimized by selecting the right material for the equipment in contact with the brine, the pressure valve and the separator for the LPT and the heater and boiler for the ORC. The materials suggested are either R316 or S32205 stainless steels. A more detailed study for material selection is recommended before taking this project further. The polymerizing silica scales in both bottoming units are considered a surmountable problem. The silica precipitates rather slowly and is highly affected by decreasing temperatures and pH values.

For the ORC, the brine is led through the tube side of the boiler and the shell side of the heater. For the optimized ORC serial setup, the temperature does not reach below 164°C in the boiler, meaning the silica scales only precipitate in the heater. The heater was chosen as a floating head tube and shell heat exchanger, having the option of being cleaned. The silica scales should be minimized and even prevented in the heat exchangers by having the brine travel at a fast rate through them. The ORC parallel setup could be more problematic and need more cleaning than the serial setup due to the lower temperature of the brine. Clogging due to silica scaling could form in the boiler in the parallel setup if the fluid travels slowly. For the optimized LPT cycle, silica will be present in the separator and possibly the turbine as well. The scales could be minimized by making the brine more acidic and delaying the formation in the separator. The silica scales would have to be cleaned when operations are down due to increased district heat demand. The precipitation of silica would also occur in the current heat exchangers used for the district heating network. That is not considered a problem due to the fact that they are already cleaned every other year.

The environmental impact from Nesjavellir geothermal CHP plant will alter with the existence of a power generating bottoming unit. As the seasonal surplus is utilized, less heat is reinjected into the shallow reservoir or disposed of above ground. For both bottoming units, a considerable amount of heat is utilized instead of possibly causing a thermal pollution in groundwater bodies located near Nesjavellir. More than 400 GWh_{th} of thermal heat from the separated brine is utilized within one year by the optimized ORC setup, see Figure 5.14. More than 300 GWh_{th} of thermal heat from the separated brine is utilized within one year by the LPT cycle, see Figure 5.20. Extra precaution must be taken to secure that the working fluid in the ORC does not leak to the environment due to a possible global warming potential. This extra precaution leads to an increased total CAPEX for the ORC. No new land is needed for the location of the possible bottoming unit.

The assumption was made for this study that when district heat demand surpasses the available heat from the bottoming unit, the operations of the bottoming unit would recede and stop completely. Another recommended approach for future work is to take into consideration that the bottoming unit could operate at a partial load, less then designed, when district heat demand increases and ceasing operation. Other recommendations before taking this project further is to improve the quality of the economic feasibility study by gathering more data and taking inflation into consideration. The results could then be verified by comparison to offers from known geothermal technology providers. Another crucial study before expanding the project is to perform measurements and experiments on different materials in direct contact with the brine in order to find out which stainless steel would be most favorable for conditions at Nesjavellir. The rate of precipitation of silica could also be investigated and some planning done to minimize the amount of scales in the surface equipment in contact with the brine. The future work is suggested to improve and hopefully underpin the results from this study, that there is an economic feasible way of exploiting the seasonal surplus available at Nesjavellir CHP plant.

References

AACE. (1997). *Cost Estimate Classification System. AACE International Recommended Practice No. 17R-97.* AACE, Inc.

Astolfi, M., Romano, M. C., Bombarda, P., & Macchi, E. (2014). Binary ORC (Organic Rankine Cycles) power plants for the exploitation of medium-low temperature geothermal sources - Part B: Techno-economic optimization. *Energy 66* , 435-446.

Axelsson, G. (2015). Lecture note from course, JAR508M - Geothermal Energy. *Utilization of Geothermal Resources*. Reykjavík: University of Iceland. Retrieved 10 2015

Bao, J., & Zhao, L. (2013). A review of working fluid and expander selections for organic Rankine cycle. *Renewable and Sustainable Energy Reviews*, 325–342.

Bejan, A., Tsatsaronis, G., & Morn, M. (1996). *Thermal Design and Optimization.* John Wiley & Sons Inc.

Bell, I. H., Wronski, J., Quoilin, S., & Lemort, V. (2014). Pure and Pseudo-pure Fluid Thermophysical Property Evaluation and the Open-Source Thermophysical Property Library CoolProp. *Industrial & Engineering Chemistry Research, Num. 53, Vol. 6*, 2498-2508.

Dickson, M. H., & Fanelli, M. (2013). *Geothermal Energy: Utilization and Technology.* UNESCO.

DiPippo, R. (2012). *Geothermal Power Plants: Principles, Applications, Case Studies and Environmental Impact.* Elsevier.

Green, D. W., & Perry, R. H. (2008). *Perry's Chemical Engineer's Handbook, 8th Edition.* New York: McGraw-Hill.

Guðmundsson, M. T. (2015). Lecture note from course, JAR508M - Geothermal Energy. *Earth's heat budget - Source of heat, heat transfer, heat transfer with convection in porous media, origin of geothermal areas*. Reykjavík: University of Iceland. Retrieved 10 2015

Guðmundsson, Y. (2016, 4). Interview with an employee of Verkís. (P. Sigurðsson, Interviewer)

Gunnarsson, I. (2012). Measurement data from ON Power. *Fluid properties and chemical composition of separated brine at Nesjavellir*. ON Power. Retrieved 4 2016

Jóhannesson, Þ., & Guðmundsson, Y. (2015). Lecture notes from course VÉL 114F - Geothermal Power Platns. *Gathering System, Cost Analysis & Development Plan and Financing*. Reykjavík: University of Iceland.

Júlíusson, B. M., Kjartansson, G., & Karlsdóttir, M. R. (2016). Information in meetings held at ON Power with authors and supervisor. Reykjavík, Iceland.

Karlsdóttir, S. N. (2012). Corrosion, Scaling and Material Selection in Geothermal Power Production. *Comprehensive Renewable Energy*, 239-257.

Kjartansson, G. (2010). *Low Pressure Flash-Steam Cycle at Hellisheiði - Selection Based on Comparison Study of Power Cycles, Utilizing Geohtermal Brine.* Bali, Indonesia: Proceedings World Geothermal Congress.

Kjartansson, G. (2015). *Niðurrennslismál á Nesjavöllum.* Reykjavík: ON Power.

Matek, B. (2016). *2016 Annual U.S. & Global Geothermal Power Production Report.* Washington DC: Geothermal Energy Association .

MATLAB. (2014). *Version 8.4.0.150421 (R2014b).* Natick, Massachusetts: The MathWorks Inc.

Papaefthimiou, V. D., Zannis, T. C., & Rogdakis, E. D. (2006). Thermodynamic study of wet cooling tower perfomance. *International Journal of Energy Research, Vol. 30*, 411-426.

Pálmason, G. (2005). *Jarðhitabók.* Reykjavík: Hið Íslenska Bókmenntafélag.

Pálsson, H. (2014). *Utilization of geothermal energy for power production - Lecture notes.* Reykjavík: University of Iceland.

Quoilin, S., Broek, M. V., Declaye, S., Pierre, D., & Lemort, V. (2013). Techno-economic survey of Organic Rankine Cycle (ORC) systems. *Renewable and Sustainable Energy Reviews*(22), 168-186.

Seider, W. D., Seader, J. D., Lewin, D. R., & Widagdo, S. (2009). *Product and Process Design Principles. Synthesis, Analysis and Evaluation. 3rd Edition.* John Wiley & Sons, Inc.

Sinnott, R. K. (2005). *Coulson & Richardson's Chemical Engineering, Vol. 6, Chemical Engineering Design.* Elsevier.

Tassew, M. (2010). Maintenance and Operational Experience Gained By Operating the Aluto Langano Geothermal Pilot Power Plant. *Proceedings World Geothermal Congress* .

Taylor, L., Siwach, S., & Krumdieck, S. (2014). *Impact of Organic Rankine Cycle Working Fluid Selection on Heat Exchanger Desing and Cost.* Auckland, New Zealand: Proceedings 36th New Zealand Geothermal Workshop.

Valdimarsson, P. (2016). Discussion about ORC units, working fluids and economic analysis. (P. Sigurðsson, Interviewer)

Zarandi, S. S., & Ívarsson, G. (2010). *A Review of Waste Water Disposal at the Nesjavellir Geothermal Power Plant.* Bali, Indonesia: Proceeding World Geothermal Congress.

I. Appendix

The pumps used for both ORC and cooling water cycle were assumed centrifugal pumps with an electric motor. The cost equations for a centrifugal pump with an electric motor is:

$$C_{pu\&em} = F_{T,pu}F_{M,pu}C_{B,pu} + F_{T,em}C_{B,em} \quad \text{(I.1)}$$

Where F_T stands for type factor, F_M material factor and C_B base cost. The base cost of a centrifugal pump is dependent on a size factor $S = Q(H)^{0.5}$, where Q is flow rate [gal/min] and H is pump head [ft]. The base cost for a centrifugal pump is:

$$C_{B,pu} = \exp\{9.2951 - 0.6019[\ln(S)] + 0.0519[\ln(S)]^2\} \quad \text{(I.2)}$$

The type factor for a centrifugal pump depends on flow rate, number of stages, pumping head and the motor. It ranges from 1 to 8.9 but was chosen as 1-1.7 for this study. The material factor depends on the type of material chosen for the pump and can vary from 1 to 9.7. The material selection depends on the corrosiveness of the fluid and was either chosen as cast steel (1,35) or duplex stainless steel (2,0), depending on the location of the pump.

The type factor for an electrical motor varies between 0.9 and 1.8, depending safety and operational speed. The $F_{T,em}$ was chosen as 1 for this study. The base cost of an electrical motor depends on the power consumption of the motor, P_C, in horsepower:

$$C_{B,em} = \exp\{5.4866 + 0.1314[\ln(P_c)] + 0.053255[\ln(P_c)]^2 + 0.028628[\ln(P_c)]^3 - 0.0035549[\ln(P_c)]^4\} \quad \text{(I.3)}$$

A material type factor, F_M, and a head factor, F_H, are taken into consideration when calculating the cost of an induced draft fan at the top of the cooling tower. The material factor was chosen as 0.6, cast aluminum, and the head factor as 1 due to low pressure difference. The base cost of the cooling tower fan is dependent on the power consumption:

$$C_{B,fan} = \exp\{6.6547 + 0.7900[\ln(P_c)]\} \quad \text{(I.4)}$$

All of the heat exchangers taken into consideration for this study were tube and shell. Different types of tube and shell heat exchangers are available. They are often categorized into 4 different types: Fixed Head, U-Tube, Floating Head and Kettle Vaporizer (Sinnott, 2005).

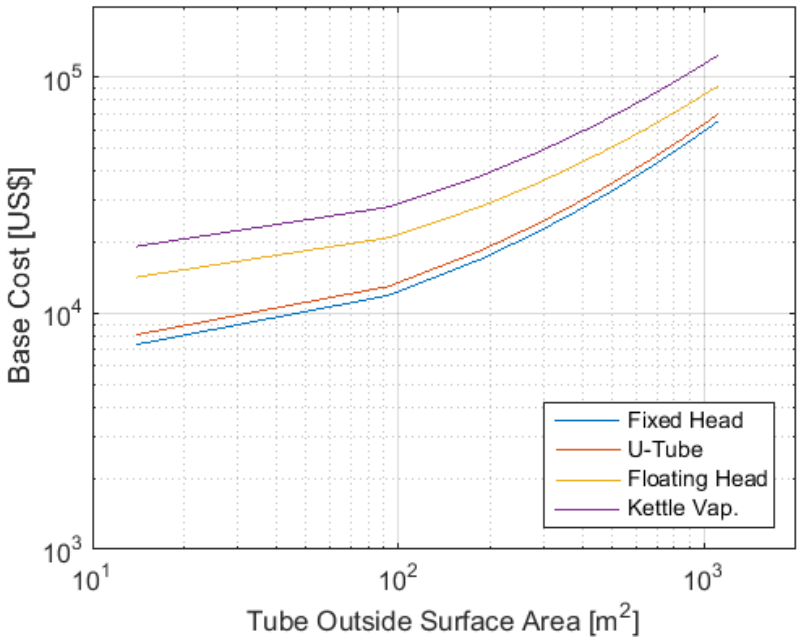

Figure I.1: Base purchase cost for the 4 types of shell and tube heat exchangers

The purchase cost of the heat exchanger take base cost C_B, a material factor F_M, a length factor F_L and a pressure factor F_P into consideration, similar to Equation (I.1). The base cost for the for different types of heat exchangers are dependent on the heat exchanging area, A [ft^2]. The area is calculated by the basic heat exchanger design equation:

$$\dot{Q} = U\ A\ \Delta T_{lm} = U\ A\ \frac{(T_{h,in} - T_{c,out}) - (T_{h,out} - T_{c,in})}{\ln\left[\frac{T_{h,in} - T_{c,out}}{T_{h,out} - T_{c,in}}\right]} \tag{I.5}$$

Where $\dot{Q}$ is the rate of heat transfer, U the overall heat transfer coefficient, A heat transfer surface area and ΔT_{lm} the log-mean temperature difference of the hot fluid and the cold fluid. The overall heat transfer coefficient depends on the fluids exchanging heat, the state of the fluids and more (Sinnott, 2005). The base cost for the different tube and shell heat exchangers are written below, where the subscripts FiH, UT, FlH and KV stand for Fixed Head, U-Tube, Floating Head and Kettle Vaporizer.

$$C_{B,FiH} = \exp\{11.0545 - 0.9228[\ln(A)] + 0.09861[\ln(A)]^2\} \tag{I.6}$$

$$C_{B,UT} = \exp\{11.147 - 0.9186[\ln(A)] + 0.09790[\ln(A)]^2\} \tag{I.7}$$

$$C_{B,FlH} = \exp\{11.667 - 0.8709[\ln(A)] + 0.09005[\ln(A)]^2\} \tag{I.8}$$

$$C_{B,KV} = \exp\{11.967 - 0.8709[\ln(A)] + 0.09005[\ln(A)]^2\} \tag{I.9}$$

The material factor, $F_{M,T\&S,}$ for tube and shell heat exchanger is also dependent on the heat transfer area, A [ft^2]:

$$F_{M,T\&S} = a + \left(\frac{A}{100}\right)^b \tag{I.10}$$

Where a ranges from 0 to 9.7 and b from 0 to 0.13, depending on the material selected for the shell side and tube side of the heat exchanger. The by choosing carbon steel at both side, the a is 0 and b 0. When choosing carbon steel at the shell side and stainless steel at the tube side, the a is 1.75 and b 0.13. With duplex stainless steel at both sides, the a is 2.7 and b 0.07. The pressure factor, $F_{P,T\&S}$, and length factor, $F_{L,T\&S}$, were assumed 1.

The cost of the throttling valve is included in the cost equation of the separator. A horizontal separator was chosen instead of a vertical one. The reason was it is cheaper mainly due to less material needed in the support structure. The cost equation for a horizontal separator is:

$$C_{sep} = F_{M,sep}C_{B,sep} + C_{S,sep} \tag{I.11}$$

Where $C_{B,sep}$ is the base cost and $C_{S,sep}$ support cost. Duplex stainless steel was chosen as material type, making the material factor to be 2.1. The base cost for a horizontal separator is dependent on the weight of the shell, We [lbs]. The weight of the horizontal separator was calculated by assuming an inner diameter, a wall thickness and knowing the density of duplex stainless steel. The weight takes the cylindrical shell and two 2:1 elliptical caps into consideration. The base cost equation is applicable with $4.2 \cdot 10^3 < We < 10^6$ and is:

$$C_{B,sep,hor} = \exp\{8.717 - 0.2330[\ln(We)] + 0.04333[\ln(We)]^2\} \tag{I.12}$$

The support cost, C_S, is dependent on the inner diameter of the separator:

$$C_{S,sep,hor} = 1.580(D_i)^{0.20294} \tag{I.13}$$

II. Appendix

The results for calculated seasonal surplus at Nesjavellir for demand in two future scenarios, 2020 and 2030. Both scenarios are simulated without the planned expansion in thermal capacity at Hellisheiði geothermal CHP plant. It is noticeable that with increasing demand and no changes to the current system, the amount of seasonal surplus available at Nesjavellir will decrease rapidly.

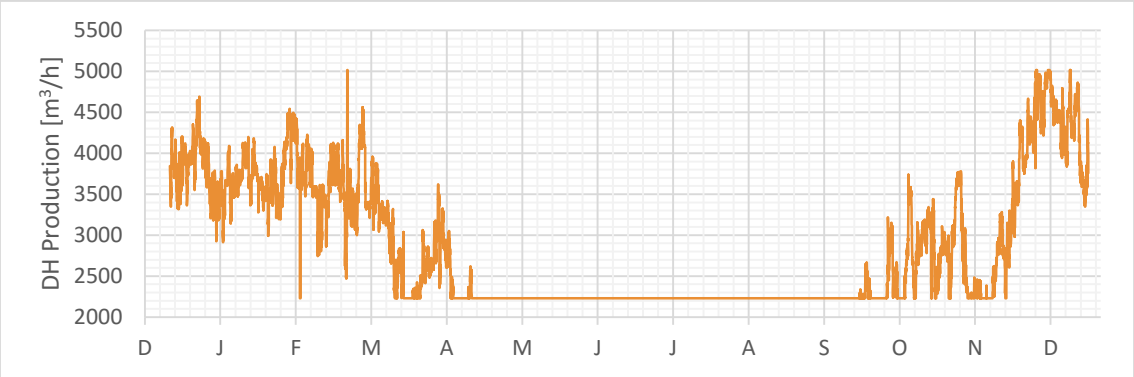

Figure II.2: Calculated district heat production at Nesjavellir in 2020 without the expansion at Hellisheiði

Figure II.3: Calculated district heat production at Nesjavellir in 2030 without the expansion at Hellisheiði

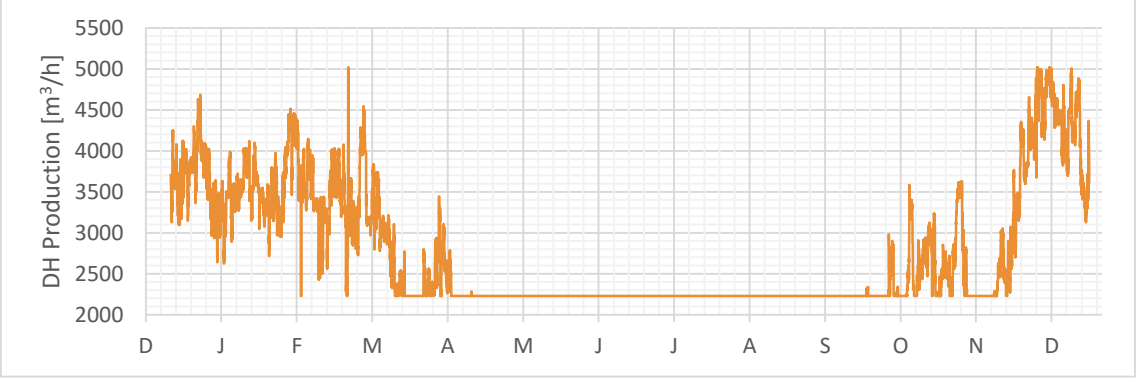

Figure II.4: Calculated district heat production at Nesjavellir in 2030 with expansion at Hellisheiði

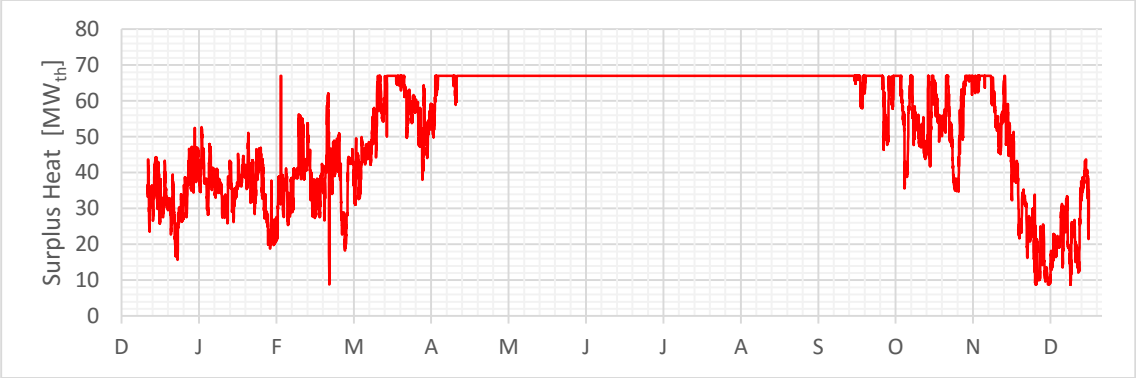

Figure II.5: Seasonal surplus at Nesjavellir in 2020 without the expansion at Hellisheiði

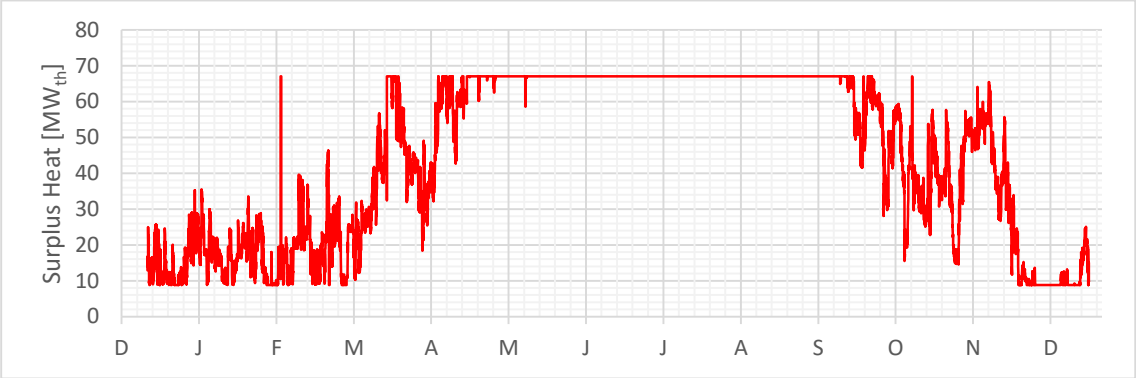

Figure II.6: Seasonal surplus at Nesjavellir in 2030 without the expansion at Hellisheiði

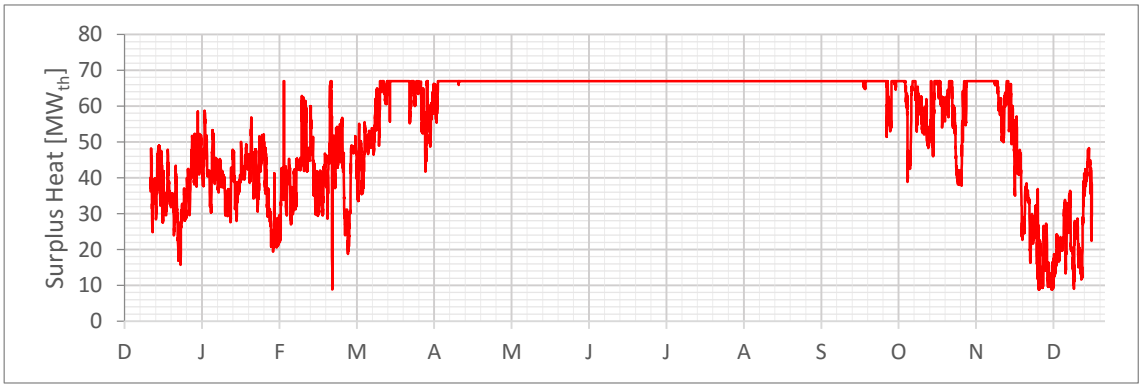

Figure II.7: Seasonal surplus at Nesjavellir in 2030 with the expansion at Hellisheiði